Mechanosensitive Rap1 activation promotes barrier function of lung vascular endothelium under cyclic stretch

Yunbo Ke[a], Pratap Karki[b], Chenou Zhang[b], Yue Li[b], Trang Nguyen[b], Konstantin G. Birukov[a], and Anna A. Birukova[b,*]

[a]Department of Anesthesiology and [b]Department of Medicine, University of Maryland School of Medicine, Baltimore, MD 21201

ABSTRACT **Mechanical ventilation remains an imperative treatment for the patients with acute respiratory distress syndrome, but can also exacerbate lung injury. We have previously described a key role of RhoA GTPase in high cyclic stretch (CS)–induced endothelial cell (EC) barrier dysfunction. However, cellular mechanotransduction complexes remain to be characterized. This study tested a hypothesis that recovery of a vascular EC barrier after pathologic mechanical stress may be accelerated by cell exposure to physiologic CS levels and involves Rap1-dependent rearrangement of endothelial cell junctions. Using biochemical, molecular, and imaging approaches we found that EC pre- or postconditioning at physiologically relevant low-magnitude CS promotes resealing of cell junctions disrupted by pathologic, high-magnitude CS. Cytoskeletal remodeling induced by low CS was dependent on small GTPase Rap1. Protective effects of EC preconditioning at low CS were abolished by pharmacological or molecular inhibition of Rap1 activity. In vivo, using mice exposed to mechanical ventilation, we found that the protective effect of low tidal volume ventilation against lung injury caused by lipopolysaccharides and ventilation at high tidal volume was suppressed in Rap1 knockout mice. Taken together, our results demonstrate a prominent role of Rap1-mediated signaling mechanisms activated by low CS in acceleration of lung vascular EC barrier restoration.**

Monitoring Editor
Alpha Yap
University of Queensland

Received: Jul 5, 2018
Revised: Jan 24, 2019
Accepted: Feb 6, 2019

INTRODUCTION

Cells and tissues within the living organism are subjected to mechanical forces in the form of shear stress (vascular endothelium), tension/compression (bone tissue), cyclic stretch (vasculature, lungs), or various grades of surrounding extracellular matrix stiffness. Mechanical forces are an indispensable part of a cell's natural microenvironment that dictate unique morphological features of the organ, organization of the cell cytoskeleton, and cell contacts with the extracellular matrix and other cells. Therefore, sensing physical forces under physiologic and pathologic conditions is a fundamental feature of living cells. Small GTPases RhoA, Rac1, and Rap1 play a key role in dynamic remodeling of the cell cytoskeleton, regulation of cellular contractility, cell responses to inflammatory insults, and control of endothelial cell (EC) permeability. Activation of RhoA stimulates EC permeability via activation of Rho-associated kinase known to directly catalyze myosin light chain (MLC) phosphorylation, or act indirectly by inactivating myosin light chain phosphatase. As a result, phosphorylation of MLC triggers actomyosin contraction, cell retraction, formation of intercellular gaps, and EC barrier compromise (Birukova *et al.*, 2004). Activation of RhoA may also positively regulate p38 MAPK and NFkB inflammatory cascades (Garcia *et al.*, 2009; Matoba *et al.*, 2010).

Emerging evidence suggests that RhoA activation may be counteracted by activation of small GTPases Rac1 and Rap1 (Birukova *et al.*, 2011a, 2013b; Tian *et al.*, 2015a). Rap1 is a member of the Ras GTPase family. Rap1 activation directly stimulates adhesion of endothelial and epithelial cells to underlying substrate and enhances cell–cell junction complexes via the Rap1 effector

This article was published online ahead of print in MBoC in Press (http://www.molbiolcell.org/cgi/doi/10.1091/mbc.E18-07-0422) on February 13, 2019.

*Address correspondence to: Anna A. Birukova (abirukova@som.umaryland.edu).

Abbreviations used: AJ, adherens junctions; ALI, acute lung injury; ARDS, acute respiratory distress syndrome; BAL, bronchoalveolar lavage; 8CPT, 8-(4-chlorophenylthio)-2′-*O*-methyl-adenosine-3′, 5′-cyclic monophosphate; CS, cyclic stretch; EC, endothelial cell; HTV, high tidal volume; ICAM1, intercellular adhesion molecule 1; LPS, lipopolysaccharides; LTV, low tidal volume; MLC, myosin light chain; MYPT, myosin phosphatase targeting protein; PBS, phosphate-buffered saline; PECAM-1, platelet endothelial cell adhesion molecule; TJs, tight junctions; TRAP6, thrombin-receptor activating peptide 6; VCAM1, vascular cell adhesion molecule 1; VEGFR2, vascular endothelial growth factor receptor 2.

protein afadin. Upon interaction with activated Rap1, afadin triggers the assembly of tight junctions (TJs) and adherens junctions (AJs; Boettner and Van Aelst, 2009), as well as physically linking TJs and AJ complexes resulting in the formation of an enhanced EC barrier (Birukova *et al.*, 2012). Rap1 may be activated by guanine nucleotide exchange factors localized at focal adhesions and cell junctions (Bos, 2005; Boettner and Van Aelst, 2009), the cell compartments known to bear mechanosensing function.

Studies testing a role of small GTPases in cell mechanosensing have been largely focused on RhoA and Rac1. It was found that in contrast to monophasic activation of Rac1 by laminar flow, regulation of Rac1 and RhoA by cyclic stretch (CS) was time and amplitude dependent. High-magnitude CS (18% CS) caused time-dependent activation of RhoA, reduction of basal Rac activity, and inhibition of lamellipodia formation (Katsumi *et al.*, 2002; Birukova *et al.*, 2006). In contrast, RhoA in endothelial cells (ECs) was not activated by physiologically relevant 5% CS (Katsumi *et al.*, 2002; Birukova *et al.*, 2006). Rap1 also participates in mechanotransduction and can be activated in ECs by shear stress leading to formation of the endothelial mechanosensing complex containing cell–cell adhesion molecules PECAM-1 and VE-cadherin associated with activated VEGFR2 (Lakshmikanthan *et al.*, 2015). A recent report demonstrated pronounced activation of Rap1 and Rap1-mediated enlargement of focal adhesions in fibroblasts exposed to a physiologically relevant magnitude of CS (Freeman *et al.*, 2017).

Vascular ECs lining the blood vessels form a semiselective barrier for macromolecules and circulating cells that is regulated by dynamic interactions between cytoskeletal elements and cell adhesion complexes. A unique feature of vascular endothelium is constant exposure to mechanical forces of various natures: shear stress by blood flow or rolling blood cells, and circumferential CS caused by heart propulsions or CS of varying amplitudes experienced by lung microvascular endothelium during physiologic lung respiratory cycles or during mechanical ventilation administered to critically ill patients. Exposure of vascular ECs to high-magnitude CS in experimental in vitro models augmented agonist-induced EC permeability (Birukov *et al.*, 2003) and activated inflammatory cytokine production (Jafari *et al.*, 2004; Yang *et al.*, 2005) and apoptosis (Pimentel *et al.*, 2001; Sanchez-Esteban *et al.*, 2002; Hammerschmidt *et al.*, 2004).

Pathologic reactions of cells and organs to excessive mechanical stimulation represent a significant clinical problem that can be best exemplified by acute respiratory distress syndrome (ARDS) affecting >200,000 patients per year in the U.S., associated with a mortality rate of 30–50% (Ware and Matthay, 2000; Rubenfeld *et al.*, 2005) and developing in critically ill patients undergoing mechanical ventilation. Mechanical ventilation of these patients is a lifesaving option; however, without precise control of ventilation volumes it can worsen or even cause de novo lung injury (Tremblay *et al.*, 1997; Ranieri *et al.*, 1999; Villar *et al.*, 2003). The landmark ARDSnet trial demonstrated a 22% decrease in ARDS mortality with the use of low tidal volume (LTV) mechanical ventilation (Goodman *et al.*, 2003). It remains unclear whether beneficial effects of LTV ventilation are due to a reduction of volutrauma caused by high tidal volume (HTV) ventilation, or whether low-magnitude mechanical strain during LTV stimulates repair mechanisms. To date, protective mechanisms activated by physiologically relevant magnitudes of mechanical strain remain virtually unexplored. Thus, mechanosensitive regulation of small GTPases and their downstream cytoskeletal targets may have important clinical implications and lead to a better understanding of the mechanisms triggering lung injury and repair in settings of mechanical ventilation.

This study tested the hypothesis that beneficial effects of LTV mechanical ventilation may be associated with stimulation of Rap1 signaling in lung vascular ECs by physiologically relevant levels of mechanical stretch. Using a cell model of human pulmonary ECs exposed to controlled levels of CS, a mouse model of lipopolysaccharide (LPS)-induced acute lung injury (ALI) with mechanical ventilation at low and high magnitudes, and a genetic model of Rap1 knockout mice, we investigated the effects of changing amplitudes of mechanical stimulation on inflammatory and permeability responses by pulmonary ECs and evaluated a role of Rap1 in cell and lung protective effects caused by application of physiologically relevant mechanical strain.

RESULTS

Effects of CS patterns on pulmonary EC cytoskeletal remodeling and activation of RhoA pathway

To investigate mechanisms of magnitude-dependent modulation of pulmonary vascular endothelial barrier function and permeability response to circulating bioactive agonists, we exposed pulmonary ECs to physiologically relevant 4% CS, high-magnitude 18% CS relevant to settings of suboptimal mechanical ventilation, or 4% CS followed by a switch to 18% CS. Human pulmonary ECs exposed to 6 h of 4% CS or 18% CS revealed similar patterns of actin cytoskeleton arrangement characterized by a circumferential F-actin rim and a few central stress fibers oriented in a perpendicular direction to the main distension vector (Figure 1A, top panels). However, immunofluorescence staining of VE-cadherin reflecting arrangement and continuity of AJs demonstrated differential effects of CS magnitudes. ECs conditioned at 4% CS demonstrated robust peripheral VE-cadherin immunoreactivity suggesting well-established, continuous AJs between neighboring ECs. In contrast, exposure to 18% CS resulted in markedly reduced VE-cadherin immunopreactivity at cell–cell junctions suggesting weakening of the EC monolayer barrier (Figure 1A, bottom panels).

Previous reports by ours and other groups showed magnitude-dependent activation of RhoA signaling in ECs exposed to CS (Kawamura *et al.*, 2003; Birukova *et al.*, 2006; Guilluy *et al.*, 2011). In agreement with published studies, 18% CS activated RhoA pathway indicated by a pronounced time-dependent increase in the levels of phosphorylated MYPT and MLC. ECs exposed to 4% CS had lower levels of phosphorylated MYPT and MLC (Figure 1B). Interestingly, ECs preconditioned at 4% CS and then exposed to 18% CS also revealed much lower levels of phosphorylated MLC than unstimulated or thrombin-stimulated cells exposed to 18% CS only (Figure 1C). These results suggest that preconditioning at physiologically relevant CS increases cell resistance to RhoA activation caused by high-magnitude CS.

EC exposure to continuous high-magnitude CS (18% CS) causes a dramatic increase in the level of thrombin-induced paracellular gap formation, as compared with thrombin-challenged ECs exposed to physiologically relevant CS magnitude (Birukov *et al.*, 2003). To investigate thrombin responses in pulmonary ECs exposed to different patterns of CS, we compared F-actin, VE-cadherin remodeling, and MLC phosphorylation in human pulmonary ECs exposed to 18% CS, 4% CS, and 4% CS followed by 18% CS and 18% CS followed by 4% CS. Because high-magnitude CS augments EC barrier-disruptive response to thrombin, in the next experiments we used thrombin at a concentration (0.05 U/ml) that causes minimal effect under static conditions. ECs continuously exposed to 18% CS developed the most robust barrier-disruptive response to thrombin challenge characterized by pronounced stress fiber formation, the appearance of paracellular gaps (Figure 2A, marked by arrows), and disruption of a continuous line of VE-cadherin immunostaining at cell junctions (Figure 2B). Interestingly, both EC preconditioning at 4% CS before the switch to 18% CS, and the

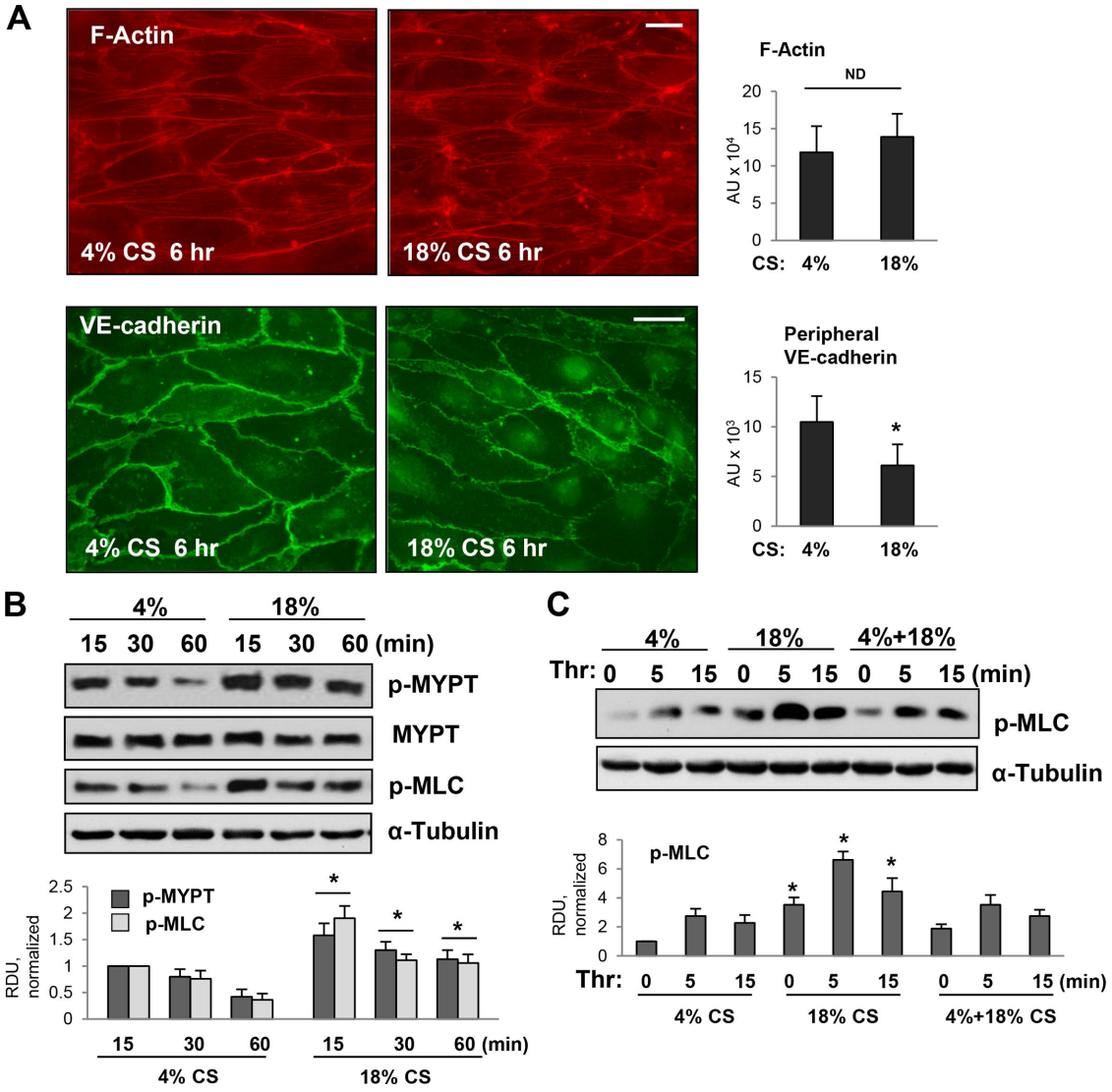

FIGURE 1: Effects of different regimens of CS on human pulmonary EC cytoskeletal remodeling and activation of RhoA pathway. (A) Effects of 4 and 18% CS on actin cytoskeleton and adherens junctions. After 6-h CS stimulation, pulmonary EC monolayers were fixed and used for immunofluorescence staining for F-actin using Texas Red phalloidin (red, top panels) and VE-cadherin antibody (green, bottom panels). Bar = 10 μm. Bar graphs represent quantitative analysis of F-actin and VE-cadherin signal intensity. Data are expressed as mean ± SD of three independent experiments, five fields per condition; *, $p < 0.05$. (B) Time course of MYPT and MLC phosphorylation in pulmonary ECs exposed to 4 and 18% CS. After CS stimulation for indicated periods of time, cells were lysed, and phosphorylation of corresponding proteins was detected by Western blot with p-MYPT1 (Thr^{850}) and pp-MLC antibodies. Equal protein loading was confirmed by membrane reprobing with α-tubulin and pan-MYPT antibodies. Bar graphs depict quantitative densitometry analysis of Western blot data; $n = 4$; *, $p < 0.05$ vs. corresponding time points from 4% CS group. (C) Time course of MLC phosphorylation in pulmonary ECs exposed to 4% CS, 18% CS, or 4–18% CS switch. Cells were exposed to 6-h 4% CS, 6-h 18% CS, or 3-h 4% CS followed by 3-h 18% CS. Thrombin stimulation was performed in the last 5–15 min of CS exposure. MLC phopshorylation was detected by Western blot with pp-MLC antibodies. Equal protein loading was confirmed by membrane reprobing with α-tubulin antibody. Bar graphs represent analysis of Western blot data; $n = 5$; *, $p < 0.05$ vs. 4% or 4–18% CS.

switch from 18% CS to 4% CS caused a less expressed barrier-disruptive response upon thrombin challenge, as compared with ECs constantly exposed to 18% CS (Figure 2, A and B).

We next used Western blot analysis of phosphorylated MLC as a reliable measure of EC contractile activation and EC barrier compromise (Birukova *et al.*, 2004). The results showed that phospho-MLC levels in thrombin-stimulated ECs subjected to CS magnitude switch were lower than in ECs exposed to continuous 18% CS (Figure 2C). Of note, the inhibitory effect of 4% CS on thrombin-induced MLC phosphorylation was less expressed in ECs subjected to an 18–4% CS switch, than in cells subjected to a 4–18% CS switch. A potential signaling mechanism associated with barrier-protective effects of low-magnitude CS was evaluated in the next experiments.

Role of Rap1 in EC AJ enhancement by low-magnitude CS

Previous studies by our group revealed a role for small GTPase Rap1 in protection against EC inflammation caused by bacterial pathogens (Birukova *et al.*, 2015) and recovery of EC barrier disruption

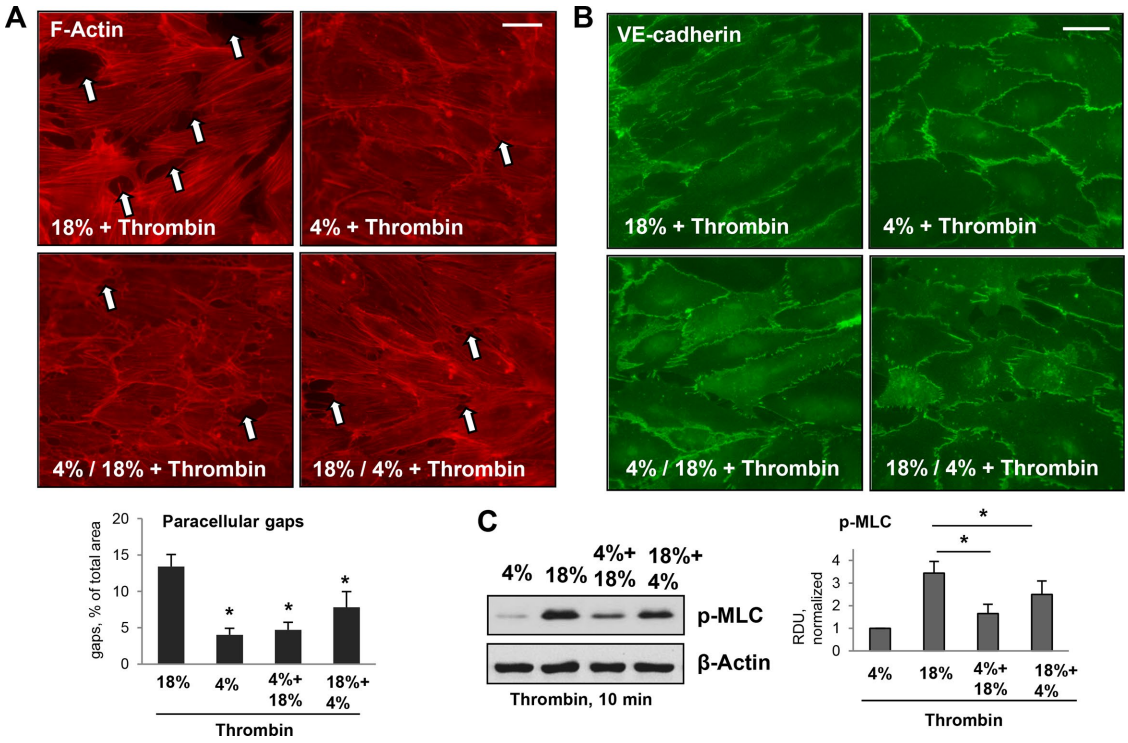

FIGURE 2: Effects of different patterns of applied CS on thrombin-induced cytoskeletal remodeling and MLC phosphorylation in human pulmonary ECs. Pulmonary ECs were treated by 18% CS or 4% CS for 6 h; alternatively, 3-h 4% CS was introduced either before or after 3-h 18% CS. Thrombin (0.05 U/ml) was added in the last 10 min of CS stimulation. (A) Visualization of F-actin using immunofluorescence staining with Texas Red phalloidin. Paracellular gaps are marked by arrows. Bar = 10 μm. Bar graphs represent quantitative analysis of gap formation. Data are expressed as mean ± SD; $n = 3$; *, $p < 0.05$. (B) Visualization of cell junctions using immunofluorescence staining with VE-cadherin antibody. Bar = 10 μm. (C) Thrombin-induced MLC phosphorylation in pulmonary ECs exposed to different patterns of CS was evaluated by Western blot with pp-MLC antibodies. Equal protein loading was confirmed by membrane reprobing with β-actin antibody. Bar graphs represent analysis of Western blot data; $n = 4$; *, $p < 0.05$.

caused by activation of intracellular contractile forces (Birukova *et al.*, 2013b). Rap1-facilitated recovery of EC monolayers integrity developed 30–60 min after activation of contractile response and resulted in the reestablishment and further enhancement of cell–cell junctions (Birukova *et al.*, 2013b). Rap1 inhibition weakened AJs and TJs in endothelial monolayers under basal conditions (Birukova *et al.*, 2009, 2012, 2013b). In the next experiments we investigated the role of Rap1 signaling in barrier-protective effects of low-magnitude CS. Analysis of Rap1 activity in EC monolayers exposed to 4% CS or 18% CS showed significant Rap1 activation in ECs exposed to 4% CS, whereas in ECs exposed to 18% CS, Rap1 activation was negligible (Figure 3A). Of note, Rap1 activation developed after 30–45 min of 4% CS stimulation suggesting a potential role of cell junction remodeling and Rap1 regulation by cell junction–associated signaling complexes.

In line with increased Rap1 activation, exposure to low-magnitude CS increased the accumulation of AJ proteins VE-cadherin and p120-catenin in the cell membrane/cytoskeletal fraction, as compared with ECs exposed to 18% CS (Figure 3B, left panels). This accumulation reflects thr increased assembly of AJprotein complexes essential for EC barrier enhancement. Remarkably, 4-h EC preconditioning at 4% CS before a switch to 18% CS increased membrane/cytoskeletal levels of VE-cadherin and p120-catenin, as compared with cells exposed to 18% CS alone. Involvement of Rap1 in 4% CS-induced membrane recruitment of VE-cadherin and p120-catenin was further evaluated using the pharmacological inhibitor of Rap1 processing, GGTI-298. Increased membrane accumulation of both AJ proteins in pulmonary ECs exposed to 4–18% CS switch, as compared with EC under 18% CS, was attenuated by pretreatment with Rap1 inhibitor (Figure 3B, right panels).

The effects of CS patterns on VE-cadherin surface expression were evaluated using a surface protein biotinylation assay as described in the *Materials and Methods* section. After in situ biotinylation of cell surface proteins in CS-stimulated cells, the level of biotinylated VE-cadherin was assessed by Western blot. We observed higher levels of biotinylated VE-cadherin in ECs subjected to 4–18% CS switch (Figure 3C). This effect was abolished in ECs pretreated with Rap1 inhibitor (Figure 3C, right panels). Molecular inhibition of Rap1 using small interfering RNA (siRNA)-induced knockdown showed similar results. Rap1 knockdown dramatically reduced the pool of biotinylated VE-cadherin in ECs exposed to 4% CS and in ECs exposed to 4% CS or to 4–18% CS switch (Figure 3D).

The results of p120-catenin VE-cadherin coimmunoprecipitation assays using p120-catenin antibody as bait were consistent with VE-cadherin surface biotinylation data and showed an increased p120-catenin–VE-cadherin association in ECs exposed to 4% CS or 4–18% CS patterns (Figure 3E, left panels). These effects were abolished by the EC pretreatment with Rap1 inhibitor (Figure 3E, right panels). Taken together, these findings are consistent with differential effects of high- and low-magnitude CS on EC monolayer barrier function.

Peripheral distribution of VE-cadherin in control and Rap1 knockdown ECs exposed to 4% CS and 18% CS was examined using immunofluorescence staining of CS-stimulated EC monolayers with VE-cadherin antibody (Figure 3F). The robust peripheral

VE-cadherin immunoreactivity in ECs exposed to 4% CS was significantly decreased by Rap1 depletion. In ECs exposed to 18% CS, Rap1 depletion caused a further disappearance of junctional VE-cadherin immunoreactivity reflecting weakening of cell junctions and more pronounced barrier failure.

The effects of Rap1 knockdown on EC barrier properties under 4% CS and 18% CS were directly tested by the permeability visualization assay previously developed in our group (Dubrovskyi *et al.*, 2013) and described in *Materials and Methods*. EC monolayers exposed to 4% CS revealed minor accumulation of fluorescein isothiocyanate (FITC)-labeled tracer at sites underlying the cell–cell junction area. Exposure to 18% CS significantly increased the EC monolayer permeability for FITC-labeled avidin (Figure 3G). Rap1 knockdown further increased EC permeability for FITC-labeled tracer in cells exposed to both 5% CS and 18% CS. The bar graph represents a quantitative analysis of EC permeability changes by measurements of the fluorescence of accumulated FITC-avidin.

Role of Rap1 mechanism in protective effects by 4% CS on thrombin-induced RhoA signaling and EC permeability

The effects of various CS patterns on thrombin-induced EC permeability were directly tested by the permeability visualization assay previously developed in our group (Dubrovskyi *et al.*, 2013) and described in *Materials and Methods*. The permeability response of EC monolayers to different CS regimens was monitored by increased accumulation of FITC-avidin on the bottoms of the biotinylated gelatin-coated wells covered by CS-stimulated EC monolayers. Exposure to 18% CS caused a significant EC permeability increase that was reflected by increased FITC-avidin accumulation underneath EC monolayers, as compared with EC exposed to more physiologically relevant 4% CS (Figure 4A, upper panels). Exposure to the 4–18% CS pattern significantly decreased permeability response by pulmonary ECs to a submaximal dose of thrombin, as compared with 18% CS conditions. This protective effect was abolished by cell pretreatment with Rap1 inhibitor GGTI-298. Visualization of FITC-avidin attached to the bottoms of the plates, and the results of quantitative analysis are presented in Figure 4A. Permeability effects were directly linked to CS effects on thrombin-induced activation of RhoA and RhoA-dependent phosphorylation of MYPT and MLC (Figure 4BC). Suppression of thrombin-induced RhoA activation, MYPT and MLC phosphorylation observed in ECs exposed to the 4–18% CS pattern was abolished by GGTI-298. Alternative inhibition of Rap1 function using siRNA-specific Rap1 protein depletion revealed similar results and showed attenuation of 4% CS and 4–18% CS protective effects against a thrombin-induced increase in MYPT and MLC phosphorylation (Figure 4D).

Attenuation of barrier-disruptive effects of 18% CS by pharmacologic stimulation of Rap1

Opposite to Rap1 inhibition, pharmacologic stimulation of Rap1 activity using a specific activator of Rap1 function, 8-(4-chlorophenylthio)-2′-*O*-methyl-adenosine-3′,5′-cyclic monophosphate (8CPT), rescued EC hyperpermeability caused by 18% CS and thrombin stimulation. Treatment with 8CPT increased peripheral VE-cadherin immunoreactivity reflecting cell junction restoration (Figure 5A) and inhibited exacerbation of thrombin-induced MYPT and MLC phosphorylation in ECs exposed to 18% CS (Figure 5B). Direct analysis of EC monolayer permeability using FITC-avidin as tracer demonstrated that EC barrier failure caused by 18% CS and thrombin was mitigated by pretreatment with 8CPT (Figure 5C). Our previous study showed an increased association of Rap1 effector, afadin, with AJ protein p120-catenin and TJ protein ZO-1, upon Rap1 activation, which resulted in a barrier-protective response by pulmonary endothelium (Birukova *et al.*, 2012). To further delineate the role of afadin in the mediation of barrier-protective effects by low-magnitude CS, we performed ectopic expression of wild-type afadin. Increased afadin expression further attenuated thrombin-induced MLC phosphorylation in ECs exposed to both high-magnitude and low-magnitude CS (Figure 5D). These results suggest a role for Rap1-dependent enhancement of cell junction integrity, which is essential for immediate barrier maintenance, as well as for down-regulation of barrier-disruptive RhoA signaling by cell junction signaling complexes.

Effects of CS magnitude switch on LPS-induced EC inflammation

Critically ill patients, including those with sepsis, depend on mechanical ventilation. To recapitulate this clinically relevant scenario of ALI in vitro, we exposed human pulmonary ECs primed with submaximal (50 ng/ml; 15 min) and maximal (200 ng/ml; 15 min) LPS doses to different patterns of CS stimulation. Exposure to 6 h of 18% CS markedly augmented EC inflammatory response to LPS reflected by increased levels of phosphorylated NFκB and increased expression of inflammatory adhesion molecules ICAM1, VCAM1, and E-selectin. Remarkably, this synergistic effect of 18% CS was abrogated in LPS-primed ECs pretreated with 4% CS (3 h) before exposure to 18% for an additional 3 h (Figure 6A). The effects of different CS patterns on LPS-induced inflammatory signaling were further evaluated by immunoflorescence analysis of NFκB nuclear translocation, an essential step for triggering inflammatory gene expression. Evident NFκB nuclear accumulation was observed in LPS-treated ECs exposed to 18% CS. In contrast, exposure to 4% CS or switch from 4% CS to 18% CS caused a marked reduction of NFκB nuclear staining caused by LPS stimulation (Figure 6B). Protective effects of 4% CS were also observed when LPS-stimulated ECs were first exposed to 18% CS, although the attenuating effect of 18–4% CS switch was less expressed. Western blot analysis of ICAM1 protein expression confirmed the immunofluorescence data and showed attenuated LPS-induced ICAM1 expression in ECs exposed to 4–18% CS switch, as compared with cells permanently exposed to 18% CS (Figure 6C). In turn, if LPS-primed ECs were first exposed to 18% CS followed by a 4% CS switch, ICAM1 expression was reduced by 18–4% CS switch in cells challenged with a submaximal LPS dose, whereas a difference in ICAM1 expression levels caused by maximal LPS concentration was negligible.

Role of Rap1 in protective effects of switch to 4% CS in two-hit model of EC inflammation

The data described above showed the role of Rap1 signaling in protective effects of 4% CS against thrombin-induced EC permeability. We next tested whether this mechanism is involved in suppression of LPS-induced inflammation caused by 4% CS switch. As shown above, high levels of ICAM1 expression in LPS-primed EC exposed to 18% CS were diminished in EC subjected to 4% CS or 4-18% CS switch. However, pretreatment with Rap1 inhibitor for 15 min before CS stimulation markedly attenuated the suppressive effects of 4% CS and abolished the effects of 4–18% CS switch on ICAM1 expression caused by a submaximal dose of LPS (Figure 7A). An alternative approach to knock down Rap1 using gene-specific siRNA showed similar results: attenuation of ICAM1 expression by 4–18% CS switch was abolished by molecular inhibition of Rap1 (Figure 7B). Conversely, activation of Rap1 signaling by small molecular activator

8CPT in EC exposed to 18% CS reduced the phospho-NFκB and ICAM1 expression to the levels comparable to LPS-treated ECs exposed to 4–18% CS switch (Figure 7C).

We next examined the effects of the CS regimen on EC cytoskeletal remodeling and barrier compromise caused by LPS. Human pulmonary ECs grown to confluence on Flexcell plates were treated with LPS (50 ng/ml) for 30 min followed by exposure to 18% CS (6 h) or 4–18% CS switch (3 h/3 h). Cytoskeletal remodeling was monitored by immunofluorescence staining for F-actin. Consistent with the protective effects described above, 4–18% CS switch induced a much lower level of EC monolayer disruption caused by LPS, manifested by a reduced number of paracellular gaps, as compared with monolayers exposed to 18% CS (Figure 7D, top panels). Importantly, siRNA-induced Rap1 knockdown further enhanced paracellular gap formation in LPS-treated ECs under 18% CS and alleviated the barrier-protective effects of 4–18% CS switch (Figure 7D, bottom panels).

The integrity of cell junctions was further monitored by double immunofluorescence staining for transmembrane AJ protein VE-cadherin. Disruption of the continuous pattern of VE-cadherin observed in LPS-primed ECs exposed to 18% CS was markedly attenuated by 4–18% CS switch (Figure 6E, top panels). This cell junction protective effect of 4–18% CS switch was abolished by Rap1 knockdown (Figure 7E, bottom panels).

Role of Rap1 mechanism in beneficial effects by LTV mechanical ventilation in the models of acute lung injury

Thrombin-receptor activating peptide (TRAP6) is a thrombin-derived nonthrombogenic peptide that serves as a PAR1 receptor ligand (Storck and Zimmermann, 1996). At submaximal dose, TRAP6 augments Rho-pathway–dependent elevation of lung vascular permeability caused by HTV mechanical ventilation without substantial activation of lung inflammation (Birukova *et al.*, 2010a; Meliton *et al.*, 2015). We used TRAP6 at submaximal dose to evaluate the effects of HTV/LTV switch on lung barrier function. Lung vascular leak in mice exposed to 4-h TRAP6/HTV or in mice exposed to 3-h TRAP6/HTV followed by switch to 1-h LTV was monitored at the end of the experiment. An Angiosense 680 EX tracer was injected intravenously, and

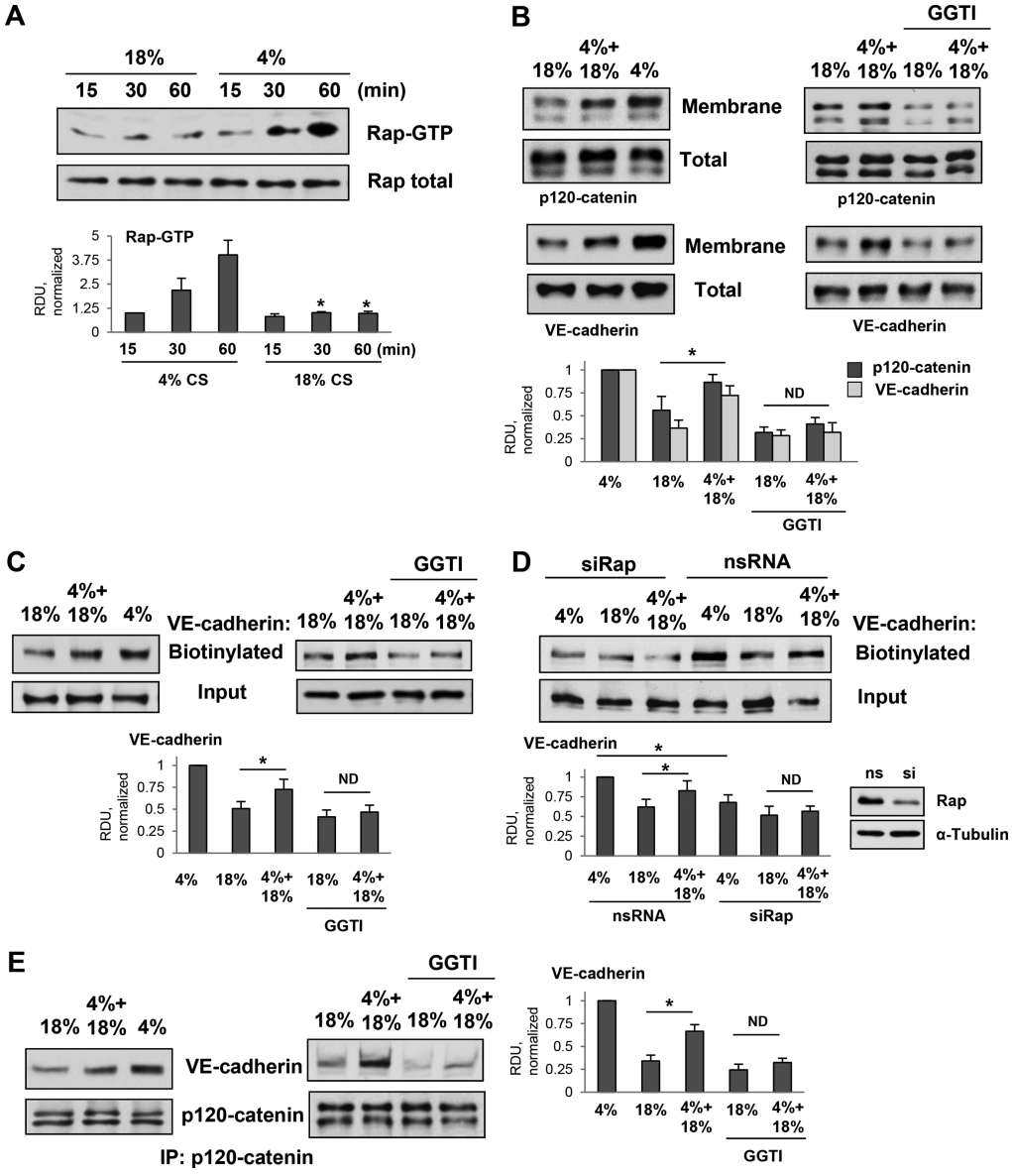

FIGURE 3: Continues.

tracer accumulation in the lungs reflecting lung vascular barrier dysfunction and lung injury was performed in anesthetized animals using the noninvasive fluorescence optical imaging approach described in *Materials and Methods*. Exposure to TRAP6/HTV caused a much higher accumulation of the fluorescent tracer in the lungs reflecting lung vascular barrier compromise, as compared with lungs exposed to 3-h TRAP6/HTV followed by switch to 1-h LTV (Figure 8A).

We further investigated modulation of inflammatory response to bacterial compounds (endotoxin) in the in vivo experiments reflecting clinical settings of patients with ALI receiving ventilation support. Exposure of mice primed with submaximal doses of LPS (0.4 mg/kg; 16 h) to 4-h HTV caused more severe lung barrier dysfunction than exposure of a similar LPS-primed group to 3-h HTV followed by 1-h LTV (Figure 8B). The results of live imaging studies were supported by

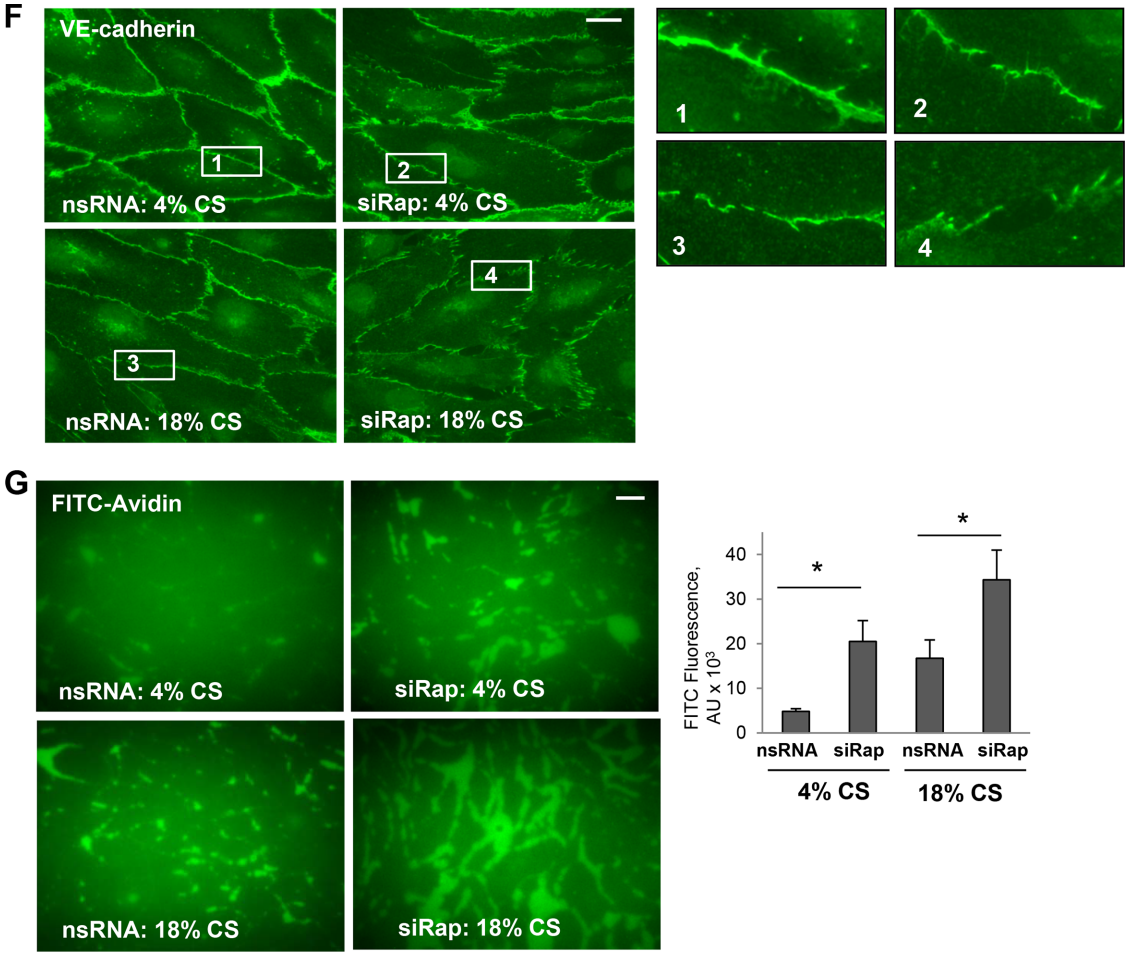

FIGURE 3: Effects of pulmonary EC exposure to different CS patterns on Rap1 activation and association between VE-cadherin and p120-catenin. (A) Time course of Rap1 activation in pulmonary ECs exposed to 18% CS or 4% CS. Pull down of GTP-bound Rap1 reflecting Rap1 activation levels was performed as described in *Materials and Methods*. Rap1 content in total cell lysates was used as a normalization control. Bar graphs represent analysis of Western blot data; $n = 4$; *, $p < 0.05$ vs. 4% CS. (B) Western blot analysis of p120-catenin and VE-cadherin content in the membrane/cytoskeletal fractions of EC exposed to 6-h 18% CS, 3-h 4% CS switched to 3-h 18% CS, or 6-h 4% CS. The content of p120-catenin and VE-cadherin in the total cell lysates was used as a normalization control. Bar graphs represent analysis of Western blot data; $n = 5$; *, $p < 0.05$. (C) HPAECs were exposed to 6-h 18% CS or 3-h 4% CS switched to 3-h 18% CS with or without pretreatment with GGTI-298 (15 μm, 30 min) before CS stimulation, and surface protein biotinylation assay was performed for VE-cadherin. VE-cadherin content in total cell lysate is presented as input. Bar graphs represent analysis of Western blot data; $n = 3$; *, $p < 0.05$. (D) HPAECs treated with nonspecific or Rap1-specific siRNA 48 h before CS stimulation were exposed to 6-h 18% CS or 3-h 4% CS switched to 3-h 18% CS. Surface protein biotinylation assay was performed for VE-cadherin. Inset demonstrates efficiency of siRNA-induced Rap1 protein depletion. Bar graphs represent analysis of Western blot data; $n = 3$; *, $p < 0.05$. (E) Coimmunoprecipitation of VE-cadherin and p120-catenin from cell lysates of ECs exposed to 6-h 18%CS, 3-h 4% CS switched to 3-h 18% CS, or 6-h 4% CS (left panel) or ECs pretreated with GGTI-298 before CS stimulation (right panel). Antibody to p120-catenin was used for immunoprecipitation. Membrane reprobing for p120-catenin was used as a normalization control. Inset shows Western blot analysis of siRNA-induced Rap1 depletion. Bar graph depicts quantitative analysis of immunoprecipitated protein complexes; $n = 4$; *, $p < 0.05$. (F) Rap1 knockdown attenuates VE-cadherin immunofluorescence at cell junctions of ECs exposed to 4% CS and promotes further disruption of VE-cadherin positive cell contacts in ECs exposed to 18%CS. Bar = 5 μm. Insets depict higher magnification images of cell junction areas. (G) Rap1 knockdown increases accumulation of FITC-avidin tracer on the substrate underlying EC monolayers. Bar = 10 μm. Bar graphs depict quantitative analysis of FITC signal expressed as mean ± SD of four independent experiments, five fields per condition; *, $p < 0.05$.

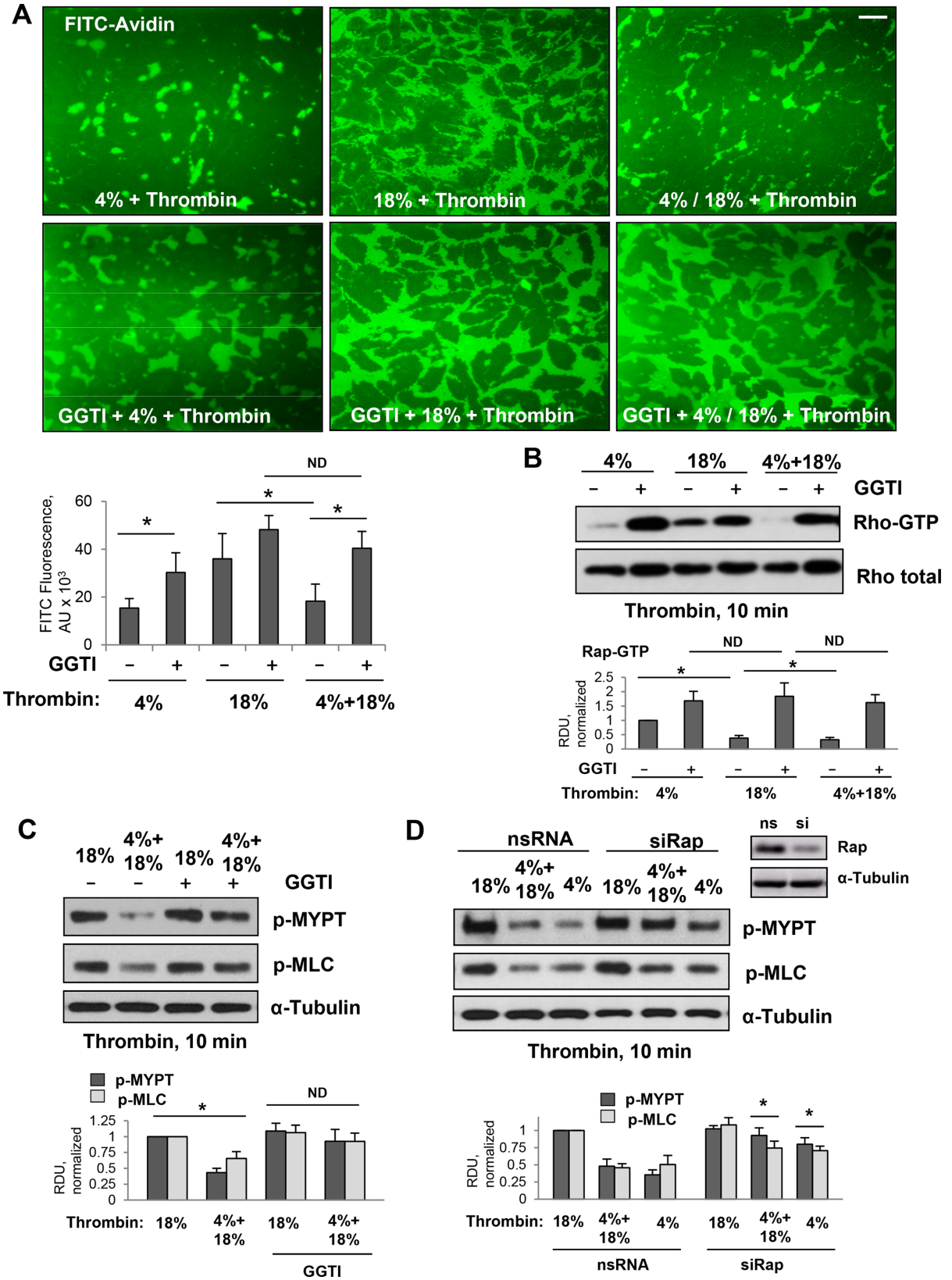

FIGURE 4: Effects of pharmacologic and molecular inhibition of Rap1 on down-regulation of Rho signaling caused by thrombin and high-magnitude CS in ECs preconditioned at 4% CS. Pulmonary ECs were exposed to 4% CS or 18% CS for 6 h, or to 3-h 4% CS switched to 3-h 18% CS. Thrombin (0.05 U/ml) was added for the last 10 min of CS experiment. Rap1 inhibitor (GGT-298, 15 μM) was added for 30 min before the 18% CS or before switching to 18% CS. (A) Visualization and quantitative analysis of FITC-avidin binding to the bottoms of the plates with CS-stimulated EC monolayers. Rap1 inhibitor attenuated 4% CS-induced protection of EC barrier integrity as detected by XPerT permeability assay. Bar = 20 μm. (B) Inhibition of Rap1 by pretreatment with GGTI-298 abolished down-regulation of

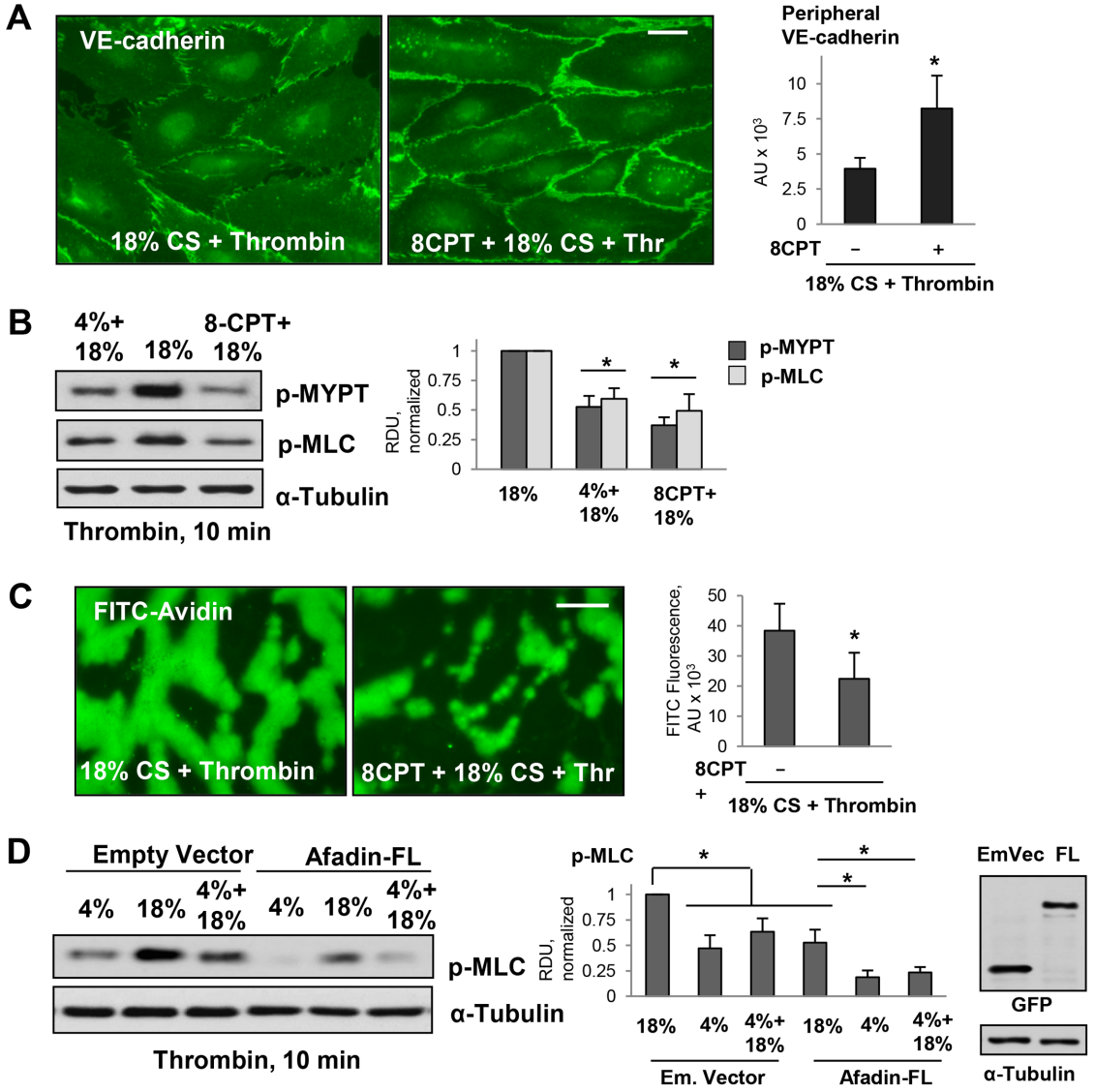

FIGURE 5: Effects of pharmacologic Rap1 activation on EC permeability in pulmonary ECs exposed to 18% CS and thrombin. (A) Pulmonary ECs were exposed to 18% CS for 6 h with or without 8CPT pretreatment (75 μM, 30 min before 18% CS) followed by thrombin stimulation (10 min). EC monolayers were then fixed and used for immunofluorescence staining with VE-cadherin antibody. Bar = 5 μm. Bar graph represents quantitative analysis of peripheral VE-cadherin signal intensity expressed as mean ± SD; $n = 4$ independent experiments; *, $p < 0.05$. (B) 18% CS-induced increase of pMYPT and pMLC levels was inhibited by 8CPT pretreatment. Bar graphs represent analysis of Western blot data; $n = 3$; *, $p < 0.05$ vs. 18% CS. (C) 18% CS-induced increase in EC permeability was inhibited by 8CPT pretreatment as detected by XPerT permeability assay; $n = 4$ independent experiments; *, $p < 0.05$. Bar = 10 μm. (D) Ectopic expression of afadin attenuated thrombin-induced MLC phosphorylation in ECs exposed to 4 and 18% CS. The ECs were transfected with empty vector or afadin plasmid (WT) 48 h before the CS stimulation. Right panel depicts protein expression of recombinant GFP-tagged afadin in pulmonary ECs. Membrane reprobing for α-tubulin was used as a normalization control. Bar graphs represent analysis of Western blot data; $n = 3$; *, $p < 0.05$.

conventional analysis of protein content and cell counts in bronchoalveolar lavage (BAL) fluid. BAL protein content and total cell count were significantly increased in LPS-primed mice exposed to 4-h HTV, as compared with 4-h LTV, but were lower in the HTV/LTV group as compared with the HTV group (Figure 8, C and D). Consistent with cell culture studies, exposure of LPS-primed mice to HTV caused higher level lung inflammatory response reflected by increased levels of inflammatory cytokines KC and MIP2, as compared with mice exposed to LTV. In turn, HTV/LTV switch attenuated KC and MIP2 production caused by priming with low dose LPS (Figure 8E).

RhoA activity caused by EC exposure to 4% CS. (C) Rap1 inhibitor attenuated suppression of RhoA-dependent phosphorylation of MYPT and MLC caused by 4% CS preconditioning. (D) Effect of siRNA-induced Rap1 knockdown on 4% CS-induced suppression of MYPT and MLC phosphorylation caused by thrombin. Right panel shows efficiency of siRNA-induced Rap1 protein depletion. Membrane reprobing for α-tubulin was used as a normalization control. Bar graphs represent analysis of Western blot data; $n = 3$; *, $p < 0.05$ vs. nonspecific RNA.

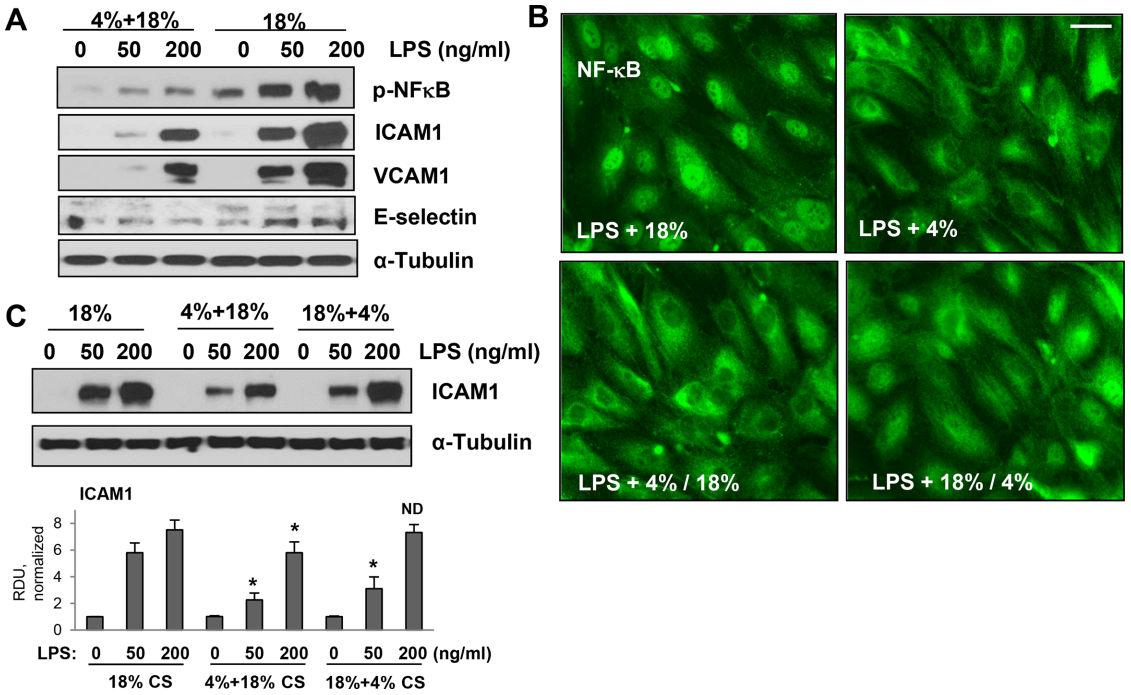

FIGURE 6: Low-magnitude CS switch attenuates inflammatory signaling activated by LPS and high-magnitude CS. Pulmonary ECs were primed by LPS for 15 min before exposure to 6-h 18% CS or 3-h 4% CS followed by 3-h 18% CS. (A) 18% CS-stimulated phosphorylation of p-NFκB and expression of ICAM1, VCAM1, and E-selectin. These effects were reduced in ECs preconditioned at 4% CS before 18% CS. (B) Intracellular localization of NFκB was detected by immunofluorescence imaging. ECs were exposed to 4% CS or to 4% CS before or after 18% CS. Bar = 10 μm. (C) Western blot analysis of ICAM1 expression. Inclusion of 4% CS before or after 18% CS reduced ICAM1 expression in pulmonary ECs activated by LPS and 18% CS. Membrane reprobing for α-tubulin was used as a normalization control. Bar graphs represent analysis of Western blot data; *, $p < 0.05$ vs. 18% CS.

RAP1 knockout attenuates protective effects of HTV/LTV switch on LPS-induced lung injury

The role of Rap1 pathway in the protective effects of HTV/LTV switch on LPS-induced lung barrier dysfunction was further investigated using a genetic model of *Rap1a–/–* mice described previously (Yan *et al.*, 2008; Birukova *et al.*, 2015). *Rap1a–/–* mice and matching controls were primed with LPS 16 h before exposure to LTV, HTV, or HTV/LTV switch. Although both the BAL protein levels and cell counts were reduced in wild-type mice exposed to HTV/LTV switch in comparison to HTV alone, this effect was abolished in *Rap1a–/–* mice (Figure 9, A and B).

The effects of Rap1a ablation on attenuation of lung injury by HTV/LTV switch were further evaluated by measurements of Evans blue extravasation into the lung tissue. Evans blue accumulation in the lung parenchyma in LPS-primed wild-type mice caused by exposure to HTV was significantly reduced by HTV/LTV switch. However, this protective effect of HTV/LTV switch was suppressed in *Rap1a–/–* mice (Figure 8C). Taken together, these results strongly suggest the role of the Rap1 mechanism in protection of lung function by HTV/LTV switch.

DISCUSSION

This study investigated the molecular mechanisms behind the differential effects of CS at physiologic and pathologic (high) magnitudes on lung endothelial barrier properties and inflammatory response by employing cellular and rodent models of varying mechanical stimulation. These in vitro and in vivo models mimic clinical settings of mechanical ventilation. The main finding of this study is a novel role of small GTPase Rap1 as a signaling hub mediating endothelial barrier-protective and anti-inflammatory effects promoted by physiologic CS levels. Our results show that, while enhanced endothelial permeability and inflammation associated with EC exposure to pathologic high-magnitude CS is driven by the activation of Rho pathway, the stimulation of Rap1 in lung vascular ECs by physiologic CS levels relevant to LTV mechanical ventilation in clinical settings counteracts Rho-mediated EC barrier disruption and inflammation. These findings posit low-magnitude ventilation as an active therapeutic strategy promoting vascular EC barrier restoration and anti-inflammatory mechanisms, rather than passive avoidance of injurious effects caused by HTV mechanical ventilation.

EC preconditioning at 4% CS caused significantly reduced Rho pathway activation and EC barrier disruption in response to thrombin, as compared with EC preconditioned at 18% CS. Moreover, thrombin-induced activation of Rho pathway, disassembly of cell junctions and gap formation was suppressed in cells preexposed to 4% CS before 18% CS and also in cells exposed to 4% CS after 18%, although to a lesser extent. Because 4% CS not only prevented 18% CS-caused endothelial disruption but also accelerated EC barrier recovery after exposure to high CS and thrombin, we further elucidated these protective mechanisms of low CS. Our previous report demonstrated that activation of Rap1 mediates the recovery of endothelial barrier function during thrombin-induced acute hyperpermeability by neutralizing barrier-disruptive effects of RhoA activation (Birukova *et al.*, 2013b). The current results show that 4% CS caused marked activation of Rap1 in a time-dependent manner. Rap1-mediated endothelial barrier recovery is facilitated by the maintenance of stable pools of AJ proteins VE-cadherin and p120-catenin in plasma membrane (Birukova *et al.*, 2007b, 2013b). In contrast, 18% CS did

not activate Rap1, but caused the loss of VE-cadherin and p120-catenin from membrane fractions. These results show that high CS disrupts this interaction that may lead to decreased endothelial barrier function. All of these AJ-disruptive events induced by 18% CS were largely repressed when 4% CS was applied to cells before undergoing 18% CS, and these protective effects were dependent on Rap1, because cells failed to show endothelial barrier recovery in the presence of pharmacological inhibitor of Rap1.

The results of this study suggest that an active cross-talk between Rap1 and Rho underlies respective barrier-protective and barrier-disruptive actions of low and high CS (Figure 4). Inhibition of Rap1 with GGTI caused a pronounced increase in thrombin-induced Rho activation even at 4% CS and abolished the Rho-inhibiting effect of 4% CS preconditioning. These observations underscore an essential role of Rap1 activation during low CS-induced endothelial barrier protection. Furthermore, the loss of protective effects of low CS preconditioning with endogenous depletion of Rap1 by siRNA and restoration with Rap1 activator 8-CPT clearly demonstrates that Rap1 is indispensable for endothelial protection by low CS preconditioning against barrier-disruptive effects of pathologically relevant high CS combined barrier-disruptive agonists.

Rap1 effector afadin plays a major role in Rap1-mediated strengthening of epithelial and endothelial AJs and TJs and EC barrier enhancement (Kooistra *et al.*, 2007; Severson and Parkos, 2009; Birukova *et al.*, 2011b; Ando *et al.*, 2013). These effects are due to structural enhancement of cell junctions via afadin-mediated integration of AJs and TJs and establishment of direct interactions between AJ and TJ proteins (Takai and Nakanishi, 2003; Ooshio *et al.*, 2010; Birukova *et al.*, 2012), as well as due to attenuation of agonist-induced RhoA pathway by the Rap1-afadin signaling axis (Birukova *et al.*, 2013b). This study shows that ectopic expression of afadin attenuated MLC phosphorylation caused by 18% CS and further augmented protective effects of 4% CS against RhoA signaling and barrier dysfunction caused by stimulation with thrombin and 18% CS. Taken together, these results suggest that EC preconditioning at low CS remodels EC monolayers, enhances monolayer integrity, and renders EC monolayer more resistant to high-magnitude CS.

In addition to thrombin that represents an acute model of endothelial dysfunction, we also took advantage of the LPS model of chronic endothelial disruption associated with inflammation to investigate whether Rap1-mediated protective effects of low CS remain functional in these settings. NFκB pathway is one of the major signaling cascades to induce inflammation in pulmonary endothelium. EC conditioning at 4% CS caused much lower levels of LPS-induced NFκB activation and expression of NFκB target genes: endothelial cell adhesion molecules ICAM1, VCAM1, and E-selectin, as compared with the cells exposed to 18% CS without low CS preconditioning. Interestingly, 18% CS-induced expression of adhesion molecules was markedly attenuated by 4% CS preconditioning. These anti-inflammatory effects of low CS preconditioning were abolished by pharmacologic or genetic inhibition of Rap1 and conversely restored with Rap1 activator, highlighting the central role of Rap1. Consistent with effects on inflammation, depletion of endogenous Rap1 augmented the LPS-induced stress fibers formation and loss of VE-cadherin at cell junctions in cells exposed to 18% CS and abolished the protective effects of 4% CS preconditioning.

Our hypothesis of protective effects of low mechanical stretch was also valid in vivo in two different models of lung injury in mechanically ventilated mice treated with TRAP6 or LPS. Both of these injurious insults led to the development of prominent lung vascular leak and inflammation in mice challenged with HTV. Introduction of LTV after HTV markedly reduced vascular leak and inflammation as evidenced by lower total inflammatory cells count, lower protein content, and reduced levels of proinflammatory cytokines KC and MIP2. LTV-induced reduction of vascular leak and inflammation was mediated by Rap1 because these protective effects were absent in Rap1 KO mice. These results strongly suggest that Rap1-mediated inhibition of inflammatory cascades and maintenance of endothelial barrier integrity played a critical role in LTV-induced protection during agonists/HTV two-hit model of lung injury; however, further studies are required to elucidate precise mechanisms of these protective effects in vivo.

How does low- and high-magnitude CS cause differential activation of RhoA- and Rap1/Rac1-mediated signaling and cell responses? This is a standing question that requires further clarification. High-magnitude CS associated with activation of RhoA pathway causes partial disassembly of peripheral microtubules and release of RhoA-specific guanine nucleotide exchange factor GEF-H1, which becomes activated in microtubule-unbound state (Birukova *et al.*, 2010b). In addition, enlargement of focal adhesion size, and activation of focal adhesion signaling by 18% CS induces MAPK-dependent targeting of GEF-H1 to paxillin and additional MAPK-dependent GEF-H1 activation at focal adhesions leading to RhoA activation, focal adhesions reinforcement, actomyosin contractility, and breach of EC barrier (Gawlak *et al.*, 2014). On the other hand, EC stimulation with low-magnitude CS caused peripheral paxillin distribution reminiscent of effects by barrier-protective agonists acting via stimulation of Rap1/Rac1 pathways (Birukova *et al.*, 2007a, 2008a,b). Indeed, EC exposed to physiologically relevant 4% CS showed increased Rap1 activity. Studies of fibroblasts exposed to unibiaxial 10% CS also showed pronounced activation of Rap1 without considerable activation of RhoA activity (Freeman *et al.*, 2017). Our experiments with ectopic expression of afadin known to integrate cell monolayers by promoting AJ and TJ interactions (Takai and Nakanishi, 2003) show attenuated MLC phosphorylation in response to thrombin in ECs exposed to 18% CS. Given the negative cross-talk relationships between RhoA and Rap1/Rac1 signaling, these results indicate that preserved cell junction integrity in EC under 4% CS may favor Rap1 activation by putative guanine nucleotide exchange factor(s) associated with cell junctions. Interestingly, applying mechanical tension to demembranized fibroblast cytoskeleton preparations caused phosphorylation of adaptor protein p130Cas and recruitment of a complex consisting of the Crk adaptor protein and Rap1-specific GEF, C3G, suggesting additional focal-adhesion–dependent mechanism of Rap1 activation by mechanical strain (Tamada *et al.*, 2004). How mechanosensitive activation of Rap1 and RhoA in these models is reciprocally regulated by CS magnitude remains to be investigated.

In summary, this is the first study describing a mechanism of low-CS-mediated protective effects in the models of pulmonary EC dysfunction in vitro and acute lung injury in vivo. On the basis of our data, we propose the following model. Exposure of pulmonary vascular endothelium to physiologically relevant CS stimulates the basal Rap1 signaling axis, which maintains the integrity of cell junctions and down-regulates barrier-disruptive and proinflammatory RhoA-NFκB signaling. Such new homeostatic state suppresses lung barrier-disruptive and inflammatory effects caused by pathologic factors such as thrombin and LPS and counteracts the augmenting effects of HTV mechanical ventilation or EC culture exposure to high-magnitude CS. These results demonstrate a role for physiologically relevant mechanical forces as an active barrier-protective and anti-inflammatory regulator of cellular signaling, rather than passive bystander, and suggest a key role for the Rap1 axis stimulated in the

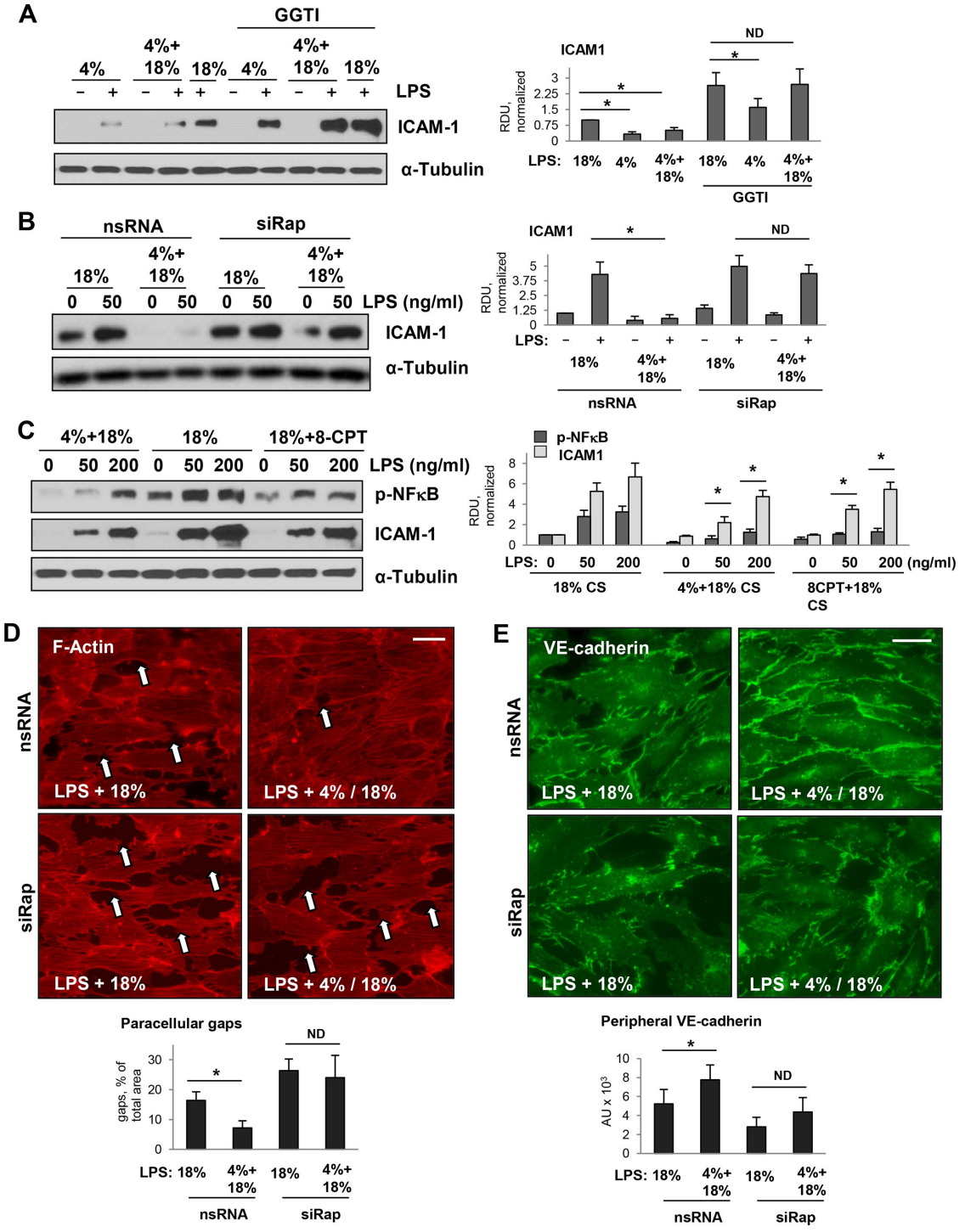

FIGURE 7: Testing protective role of Rap1 in clinically relevant cell models of ALI: inflammatory stimulation combined with exposure to CS. Pulmonary ECs were primed by LPS for 15 min followed by exposure to 4% CS, 18% CS, or 4–18% CS switch. ICAM1 expression monitored by Western blot analysis of cell lysates was used as a marker of EC inflammatory activation. (A) 4% CS attenuated ICAM1 expression caused by LPS priming and initial exposure to 18% CS, as determined by Western blot. Preincubation with Rap1 inhibitor abolished inhibitory effects of 4% CS on ICAM1 expression. (B) Knockdown of Rap1 using gene-specific siRNA attenuated the inhibitory effect of 4% CS preconditioning on expression of ICAM stimulated by LPS and 18% CS, as determined by Western blot. (C) EC primed with LPS for 15 min were treated with vehicle or Rap1 activator 8CPT (75 μM, 30 min) followed by exposure to 18% CS. Phospho-NFκB and ICAM1 levels were analyzed by Western blot as parameters of EC inflammation. For all experiments, membrane reprobing for α-tubulin was used as a normalization control. Bar graphs represent analysis of Western blot data; $n = 3$; *, $p < 0.05$ vs. 18% CS. (D) Immunofluorescence analysis of effects of 18% CS and switch from 4% CS to 18% CS on actin cytoskeleton, adherens junctions, and EC barrier disruption in LPS-primed ECs. F-actin remodeling was evaluated by immunofluorescence staining with Texas Red phalloidin. Formation of paracellular gaps (marked by arrows) was

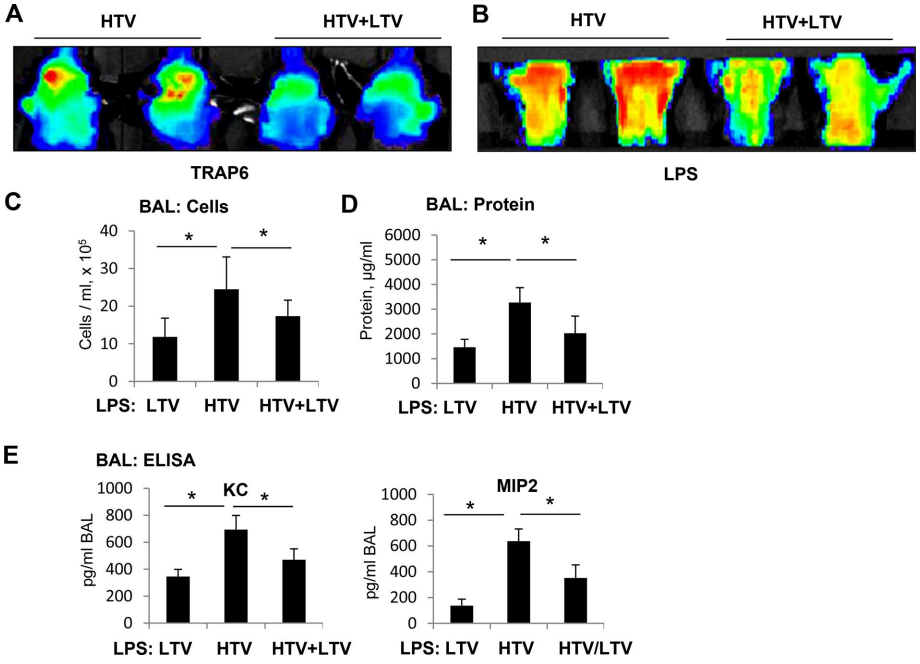

FIGURE 8: Effect of switch from HTV to LTV on parameters of LPS-induced lung injury. C57B6 WT mice were subjected to 4-h HTV, 4-h LTV, or a switch of 1-h HTV to 3-h LTV in the presence or absence of concurrent administration of TRAP6 or in the presence or absence of 18-h LPS treatment by intratracheal infusion before ventilation procedures. (A) Live imaging analysis of lung vascular leak after intravenous injection of TRAP6 and different ventilation schemes. TRAP6-induced accumulation of fluorescent Angiosense 680 EX imaging agent in the lungs was detected by a Xenogen IVIS 200 Spectrum imaging system after termination of mechanical ventilation as described in *Materials and Methods* and presented in arbitrary colors. (B) Live imaging analysis of lung vascular leak after intratracheal injection of LPS and different ventilation schemes. (C, D) Mice exposure to LTV (4 h), HTV (4 h), or HTV (1 h)-LTV (3 h) switch was performed 18 h after LPS administration (intratracheal). At the end of experiment, BAL collection was performed, and measurements of total cell count (C) and protein concentration (D) were performed in BAL samples. (E) The BAL levels of the mouse KC and MIP2 were evaluated using ELISA. Data are expressed as mean ± SD of four independent experiments; *, $p < 0.05$ vs. LPS alone.

lung by physiologic mechanical stretch in propagation of ALI recovery and restoration of lung endothelial barrier.

MATERIALS AND METHODS

Cell culture and reagents

Human pulmonary artery endothelial cells (HPAECs) were obtained from Lonza (Allendale, NJ) and used at passages 5–8. All experiments were performed in EGM growth medium (Lonza) containing 2% fetal bovine serum (FBS) unless otherwise specified. Texas Red–conjugated phalloidin and Alexa Fluor 488–labeled secondary antibodies were purchased form Molecular Probes (Eugene, OR). TRAP6 was obtained from AnaSpec (San Jose, CA). 8CPT was obtained from Calbiochem (La Jolla, CA). GGTI-298 and thrombin were obtained from Millipore-Sigma. Antibodies to diphospho–myosin light chain (MLC), pan-MLC, MYPT, pMYPT, p120-catenin, phospho-NFκB, β-actin, and tubulin antibodies were obtained from Cell Signaling (Beverly, MA); Rap1, VE-cadherin, ICAM1, VCAM1, and E-selectin antibodies were from Santa Cruz Biotechnology (Santa Cruz, CA). HRP-linked anti-mouse and anti-rabbit IgG were obtained from Cell Signaling (Beverly, MA). Unless otherwise specified, all biochemical reagents were obtained from Sigma (St. Louis, MO).

Cell culture under CS

CS experiments were performed according to the previously described protocol (Birukov *et al.*, 2003; Shikata *et al.*, 2005) using the FX-4000T Flexcell Tension Plus system (Flexcell; McKeesport, PA) equipped with a 25-mm BioFlex Loading station. Experiments were performed in the presence of culture medium containing 2% FBS. HPAEC were seeded at standard densities (8×10^5 cells/well) onto collagen I–coated flexible bottom BioFlex plates. Both static HPAEC cultures and cells exposed to CS were seeded onto identical plates to ensure standard culture conditions. After 48 h of culture, cells were exposed to desired periods of high-magnitude (18% linear elongation, sinusoidal wave, 25 cycles/min) or low-magnitude (4% linear elongation, sinusoidal wave, 25 cycles/min) CS, or CS magnitude was switched during experiment. Control BioFlex plates with static EC culture were placed in the same cell culture incubator and processed similarly to CS-preconditioned cells. At the end of experiments, cell lysates were collected for RhoA activation assays, Western blot analysis, or CS-exposed endothelial monolayers were fixed and used for immunofluorescence staining.

Immunofluorescence staining and image analysis

Following CS exposure and agonist stimulation, ECs were fixed in 3.7% formaldehyde solution in phosphate-buffered saline (PBS) for 10 min at 4°C, washed with PBS, permeabilized with 0.1% Triton X-100 in PBS for 30 min at room temperature, and blocked with 2% bovine serum albumin (BSA) in PBS for 30 min. Incubation with an antibody of interest was performed in blocking solution (2% BSA in PBS) for 1 h at room temperature followed by staining with Alexa 488–conjugated secondary antibodies. Actin filaments were stained

observed in LPS-primed ECs exposed to 18% CS (6 h). Disruption of EC monolayers was attenuated in LPS-primed ECs preconditioned at 4% CS (3 h) before 18% CS switch (3 h). Bar graph depicts quantitative analysis of gap formation; $n = 3$; *, $p < 0.05$. Knockdown of Rap1 using gene-specific siRNA attenuated the protective effect of 4% CS preconditioning on monolayer integrity. Bar = 10 µm. (E) Immunofluorescence analysis of VE-cadherin at the cell junctions in pulmonary ECs primed with LPS. Left two panels: 18% CS; right two panels: switch from 4% CS to 18% CS. Bar = 10 µm. Bar graphs show quantitative analysis of VE-cadherin signal intensity. Data are expressed as mean ± SD of three independent experiments, five fields per condition; *, $p < 0.05$.

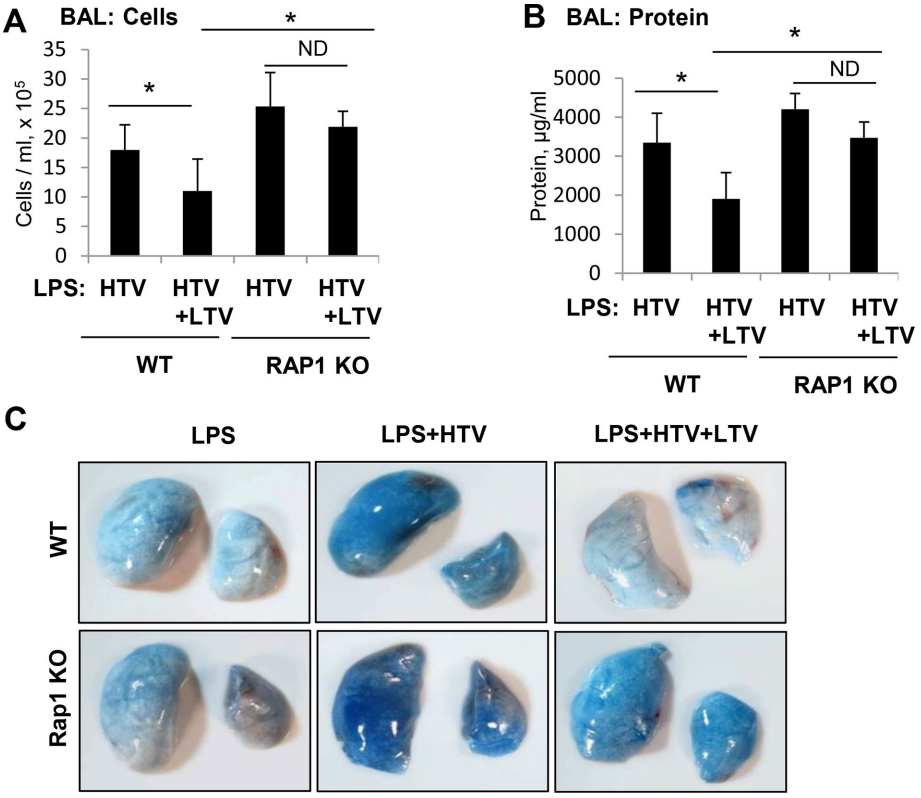

FIGURE 9: Role or Rap1 in the protective effect of HTV-LTV switch on LPS-induced lung injury. LPS administration (intratracheal) of *Rap1–/–* mice and matched wild-type controls was performed 18 h before exposure to different regimens of mechanical ventilation. The experiment was terminated after 4 h of mechanical ventilation. (A) BAL cell count measurements. (B) BAL protein content measurements. Data are expressed as mean ± SD of four independent experiments; *, $p < 0.05$. (C) Evans blue dye (30 ml/kg, i/v) was injected 30 min before termination of the experiment. Photographs depict lung vascular permeability assessed by Evans blue accumulation in the lung tissue.

with Texas Red–conjugated phalloidin diluted in the blocking solution. After immunostaining, the elastic membranes with cells were excised from the BioFlex plates and placed on large coverslips, and immunofluorescence imaging was performed using an inverted microscope Nikon Eclipse TE300 connected to a SPOT RT monochrome digital camera and image processor (Diagnostic Instruments, Sterling Heights, MI). The images were processed with Adobe Photoshop 7.0 (Adobe Systems, San Jose, CA).

Coimmunoprecipitation, differential protein fractionation, and immunoblotting

After agonist stimulation, cells were harvested and lysed with cold TBS-NP40 lysis buffer (20 mM Tris, pH 7.4, 150 mM NaCl, 1% NP40) supplemented with protease and phosphatase inhibitor cocktails (Roche, Indianapolis, IN). Clarified lysates were then incubated with antibodies to VE-cadherin overnight at 4°C, washed three to four times with TBS-NP40 lysis buffer, and the complexes were analyzed by Western blotting using appropriate antibodies (Tian *et al.*, 2015b). In fractionation studies, cytosolic (soluble) and membrane/cytoskeletal (particulate) fractions were isolated as described previously (Birukova *et al.*, 2007b). Protein extracts were separated by SDS–PAGE, transferred to polyvinylidene fluoride (PVDF) membrane, and probed with specific antibodies. Equal protein loading was verified by reprobing membranes with antibody to β-actin or a specific protein of interest.

Surface protein biotinylation was performed as previously described (Birukova *et al.*, 2013a) with some modifications. Briefly, after exposure to CS and/or agonist stimulation, cells were washed with PBS at 37°C and incubated for 10 min with 5 mM sulfo-NHS-SS-biotin (Pierce Biotechnology, Rockford, IL) at RT. Subsequently, cells were washed two times with ice-cold PBS with 100 mM glycine, lysed for 30 min on ice in 1% Triton-100 PBS, and cell lysate centrifuged at 10,000 × *g* for 10 min at 4°C. Equal amounts of cell lysates were incubated with 60 µl of streptavidin-agarose (Pierce Biotechnology, Rockford, IL) for 1 h at 4°C. Beads were washed three times with ice-cold PBS and boiled in SDS sample buffer with 5% 2-mercaptoethanol. Samples were centrifuged for 1 min at 1000 × *g*, and supernatants were subjected to Western blot analysis with VE-cadherin antibody.

DNA and siRNA transfections

Predesigned Rap1A-specific human Stealth Select siRNA set of standard purity was ordered from Invitrogen (Carlsbad, CA). Transfection of ECs with siRNA was performed as previously described (Singleton *et al.*, 2009). Nonspecific, nontargeting siRNA was used as a control treatment. After 48 h of transfection, cells were used for experiments or harvested for Western blot verification of specific protein depletion. Plasmid encoding wild-type afadin bearing GFP tag was kindly provided by Y. Takai (Kobe University, Japan) and used for transient transfections according to protocol described previously (Birukova *et al.*, 2010b). Control transfections were performed with empty vectors. After 24–48 h of transfection, cells were treated with an agonist of interest and used for permeability measurements or subjected to immunofluorescence analysis.

Rap1 activation assay was performed using commercially available assay kits purchased from Upstate Biotechnology (Lake Placid, NY). In brief, cells after exposure to different CS conditions for various periods of time were lysed on ice, and GTP-bound Rap1 was captured using pull-down assays with Ral GDS-RBD agarose, according to the manufacturer's protocols. The levels of activated GTP-Rap1 as well as total Rap1 were evaluated by Western blot analysis.

Permeability measurements in CS-conditioned EC monolayers

Endothelial permeability to macromolecules was monitored by express permeability testing assay (XPerT; Dubrovskyi *et al.*, 2013) available from Millipore (cat. #17-10398). For the permeability assay, cells were seeded on biotinylated gelatin-coated BioFlex plates and grown for 48–72 h before exposure to desired CS conditions and agonist stimulation. FITC-avidin solution was added directly to the culture medium at the final concentration 25 µg/ml for 3 min before termination of the experiment unless otherwise specified. Unbound FITC-avidin was washed out with 200 µl PBS, pH 7.4, 37°C (two cycles, 10 s each). Then, elastic bottoms were excised from of BioFlex plates and placed

in cuvettes containing 200 µl PBS. The fluorescence of matrix-bound FITC-avidin was measured on a Victor X5 Multilabel Plate Reader (Perkin Elmer, Waltham, MA) using an excitation wavelength of 485 nm and emission wavelength of 535 nm.

Animal studies and mechanical ventilation protocol

All animal care and treatment procedures were approved by the University of Maryland and University of Chicago Institutional Animal Care and Use Committees. C57Bl/6j mice (8–10 wk old) were purchased from Jackson Laboratories (Bar Harbor, ME). Animals were handled according to the National Institutes of Health Guide for the Care and Use of Laboratory Animals. *Rap1a−/−* mice have been described elsewhere (Yan *et al.*, 2008; Birukova *et al.*, 2015). C57BL/6J mice were purchased from Jackson Laboratories (Bar Harbor, ME). Male and female mice, 8–10 wk old, with an average weight 20–25 g (Jackson Laboratories, Bar Harbor, ME) were anesthetized with an intraperitoneal injection of ketamine (75 mg/kg) and acepromazine (1.5 mg/kg). A tracheotomy was performed and the trachea was cannulated with a 20-gauge 1-inch catheter, which was tied into place to prevent air leakage. The animals were placed on a mechanical ventilator (Harvard Apparatus, Boston, MA). Mice were randomized to concurrently receive a single dose of TRAP6 (1.5×10^{-5} mol/kg; intratracheal instillation) or LPS (0.75 mg/kg body wt; *Escherichia coli* O55:B5) followed by 4 h of mechanical ventilation with HTV (30 ml/kg, 75 breaths per minute and 0 PEEP, HTV), LTV (7 ml/kg, 100 breaths per minute and 0 PEEP, HTV), or their combination. Control animals were anesthetized and allowed to breathe spontaneously. At killing, BAL of both lungs was performed with 1 ml of sterile Hanks' balanced salt solution for measurement of inflammatory cells and protein.

Evaluation of lung injury parameters

At killing, collection of BAL fluid was performed using 1 ml of sterile Hanks' balanced saline buffer. The BAL protein concentration was determined by a BCATM Protein Assay kit (Thermo Scientific, Pittsburg, PA). BAL inflammatory cell counting was performed using a standard hemacytometer technique (Fu *et al.*, 2009). As an additional parameter reflecting increased lung vascular leakiness, Evans blue accumulation in the lung tissue was evaluated as described elsewhere (Fu *et al.*, 2009). At the end of the experiment, a thoracotomy was performed, and the lungs were perfused in situ via the left atrium with PBS containing 5 mM EDTA to flush the blood off the lungs. The left lung and right lung were excised and imaged by a Kodak digital camera.

Optical imaging of lung vascular leak in vivo

Mice were injected via tail vein with 100 µl of 2 nM Angiosense 680 EX (a vascular fluorescent blood pool imaging agent; PerkinElmer, Inc., Boston, MA; cat# NEV10054EX). After 24 h, fluorescent optical imaging was performed using Xenogen IVIS 200 Spectrum (Caliper Life Sciences. Alameda, CA). Mice were exposed to isoflurane anesthesia with O_2 through the gas anesthesia manifold and placed on the imaging stage. Acquisition and image analysis were performed with Living Image 4.3.1 software as we have previously described (Birukova *et al.*, 2015).

Measurement of cytokines

The concentrations of KC and MIP2 in mouse BAL fluid samples were measured using mouse-specific enzyme-linked immunosorbent assay (ELISA) kits available from R&D Systems (Minneapolis, MN) according to manufacturer's instructions. Absorbance was read at 450 nm within 30 min in a Victor X5 Multilabel Plate Reader (Perkin Elmer, Waltham, MA). Standard curves were generated with an expected minimum detectable concentration of 8 pg/ml.

Statistical analysis

Results are expressed as means ± SD of three to five independent experiments. Stimulated samples were compared with controls by unpaired Student's *t* test. For multiple-group comparisons, one-way analysis of variance (ANOVA) followed by the post hoc Fisher's test were used. $p < 0.05$ was considered statistically significant.

ACKNOWLEDGMENTS

This work was supported by grants HL076259, HL087823, HL107920, and HL130431 from the National Heart, Lung, and Blood Institute; AG048231 from the National Institute on Aging; and GM122940 and GM114171 from the National Institute of General Medical Sciences.

REFERENCES

Ando K, Fukuhara S, Moriya T, Obara Y, Nakahata N, Mochizuki N (2013). Rap1 potentiates endothelial cell junctions by spatially controlling myosin II activity and actin organization. J Cell Biol 202, 901–916.

Birukov KG, Jacobson JR, Flores AA, Ye SQ, Birukova AA, Verin AD, Garcia JG (2003). Magnitude-dependent regulation of pulmonary endothelial cell barrier function by cyclic stretch. Am J Physiol Lung Cell Mol Physiol 285, L785–L797.

Birukova AA, Alekseeva E, Cokic I, Turner CE, Birukov KG (2008a). Cross talk between paxillin and Rac is critical for mediation of barrier-protective effects by oxidized phospholipids. Am J Physiol Lung Cell Mol Physiol 295, L593–L602.

Birukova AA, Chatchavalvanich S, Rios A, Kawkitinarong K, Garcia JG, Birukov KG (2006). Differential regulation of pulmonary endothelial monolayer integrity by varying degrees of cyclic stretch. Am J Pathol 168, 1749–1761.

Birukova AA, Cokic I, Moldobaeva N, Birukov KG (2008b). Paxillin is involved in the differential regulation of endothelial barrier by HGF and VEGF. Am J Respir Cell Mol Biol 40, 99–107.

Birukova AA, Fu P, Wu T, Dubrovskyi O, Sarich N, Poroyko V, Birukov KG (2012). Afadin controls p120-catenin-ZO-1 interactions leading to endothelial barrier enhancement by oxidized phospholipids. J Cell Physiol 227, 1883–1890.

Birukova AA, Fu P, Xing J, Birukov KG (2009). Rap1 mediates protective effects of iloprost against ventilator induced lung injury. J Appl Physiol 107, 1900–1910.

Birukova AA, Fu P, Xing J, Cokic I, Birukov KG (2010a). Lung endothelial barrier protection by iloprost in the 2-hit models of ventilator-induced lung injury (VILI) involves inhibition of Rho signaling. Transl Res 155, 44–54.

Birukova AA, Fu P, Xing J, Yakubov B, Cokic I, Birukov KG (2010b). Mechanotransduction by GEF-H1 as a novel mechanism of ventilator-induced vascular endothelial permeability. Am J Physiol Lung Cell Mol Physiol 298, L837–L848.

Birukova AA, Malyukova I, Poroyko V, Birukov KG (2007a). Paxillin-β-catenin interactions are involved in Rac/Cdc42-mediated endothelial barrier-protective response to oxidized phospholipids. Am J Physiol Lung Cell Mol Physiol 293, L199–L211.

Birukova AA, Meng F, Tian Y, Meliton A, Sarich N, Quilliam LA, Birukov KG (2015). Prostacyclin post-treatment improves LPS-induced acute lung injury and endothelial barrier recovery via Rap1. Biochim Biophys Acta 1852, 778–791.

Birukova AA, Smurova K, Birukov KG, Kaibuchi K, Garcia JGN, Verin AD (2004). Role of Rho GTPases in thrombin-induced lung vascular endothelial cells barrier dysfunction. Microvasc Res 67, 64–77.

Birukova AA, Starosta V, Tian X, Higginbotham K, Koroniak L, Berliner JA, Birukov KG (2013a). Fragmented oxidation products define barrier disruptive endothelial cell response to OxPAPC. Transl Res 161, 495–504.

Birukova AA, Tian X, Tian Y, Higginbotham K, Birukov KG (2013b). Rap-afadin axis in control of Rho signaling and endothelial barrier recovery. Mol Biol Cell 24, 2678–2688.

Birukova AA, Zagranichnaya T, Alekseeva E, Fu P, Chen W, Jacobson JR, Birukov KG (2007b). Prostaglandins PGE2 and PGI2 promote

endothelial barrier enhancement via PKA- and Epac1/Rap1-dependent Rac activation. Exp Cell Res 313, 2504–2520.
Birukova AA, Zebda N, Cokic I, Fu P, Wu T, Dubrovskyi O, Birukov KG (2011a). p190RhoGAP mediates protective effects of oxidized phospholipids in the models of ventilator-induced lung injury. Exp Cell Res 317, 859–872.
Birukova AA, Zebda N, Fu P, Poroyko V, Cokic I, Birukov KG (2011b). Association between adherens junctions and tight junctions via Rap1 promotes barrier protective effects of oxidized phospholipids. J Cell Physiol 226, 2052–2062.
Boettner B, Van Aelst L (2009). Control of cell adhesion dynamics by Rap1 signaling. Curr Opin Cell Biol 21, 684–693.
Bos JL (2005). Linking Rap to cell adhesion. Curr Opin Cell Biol 17, 123–128.
Dubrovskyi O, Birukova AA, Birukov KG (2013). Measurement of local permeability at subcellular level in cell models of agonist- and ventilator-induced lung injury. Lab Invest 93, 254–263.
Freeman SA, Christian S, Austin P, Iu I, Graves ML, Huang L, Tang S, Coombs D, Gold MR, Roskelley CD (2017). Applied stretch initiates directional invasion through the action of Rap1 GTPase as a tension sensor. J Cell Sci 130, 152–163.
Fu P, Birukova AA, Xing J, Sammani S, Murley JS, Garcia JG, Grdina DJ, Birukov KG (2009). Amifostine reduces lung vascular permeability via suppression of inflammatory signalling. Eur Respir J 33, 612–624.
Garcia MC, Ray DM, Lackford B, Rubino M, Olden K, Roberts JD (2009). Arachidonic acid stimulates cell adhesion through a novel p38 MAPK-RhoA signaling pathway that involves heat shock protein 27. J Biol Chem 284, 20936–20945.
Gawlak G, Tian Y, O'Donnell JJ, 3rd, Tian X, Birukova AA Birukov KG (2014). Paxillin mediates stretch-induced Rho signaling and endothelial permeability via assembly of paxillin-p42/44MAPK-GEF-H1 complex. FASEB J 28, 3249–3260.
Goodman RB, Pugin J, Lee JS, Matthay MA (2003). Cytokine-mediated inflammation in acute lung injury. Cytokine Growth Factor Rev 14, 523–535.
Guilluy C, Swaminathan V, Garcia-Mata R, O'Brien ET, Superfine R, Burridge K (2011). The Rho GEFs LARG and GEF-H1 regulate the mechanical response to force on integrins. Nat Cell Biol 13, 722–727.
Hammerschmidt S, Kuhn H, Grasenack T, Gessner C, Wirtz H (2004). Apoptosis and necrosis induced by cyclic mechanical stretching in alveolar type II cells. Am J Respir Cell Mol Biol 30, 396–402.
Jafari B, Ouyang B, Li LF, Hales CA, Quinn DA (2004). Intracellular glutathione in stretch-induced cytokine release from alveolar type-2 like cells. Respirology 9, 43–53.
Katsumi A, Milanini J, Kiosses WB, delPozo MA, Kaunas R, Chien S, Hahn KM, Schwartz MA (2002). Effects of cell tension on the small GTPase Rac. J Cell Biol 158, 153–164.
Kawamura S, Miyamoto S, Brown JH (2003). Initiation and transduction of stretch-induced RhoA and Rac1 activation through caveolae: cytoskeletal regulation of ERK translocation. J Biol Chem 278, 31111–31117.
Kooistra MR, Dube N, Bos JL (2007). Rap1: a key regulator in cell-cell junction formation. J Cell Sci 120, 17–22.
Lakshmikanthan S, Zheng X, Nishijima Y, Sobczak M, Szabo A, Vasquez-Vivar J, Zhang DX, Chrzanowska-Wodnicka M (2015). Rap1 promotes endothelial mechanosensing complex formation, NO release and normal endothelial function. EMBO Rep 16, 628–637.
Matoba K, Kawanami D, Ishizawa S, Kanazawa Y, Yokota T, Utsunomiya K (2010). Rho-kinase mediates TNF-α-induced MCP-1 expression via p38 MAPK signaling pathway in mesangial cells. Biochem Biophys Res Commun 402, 725–730.
Meliton A, Meng F, Tian Y, Shah A, Birukova AA, Birukov KG (2015). KRIT1 mediates prostacyclin-induced protection against lung vascular permeability induced by excessive mechanical forces and TRAP6. Am J Respir Cell Mol Biol 53, 10.1165/rcmb.2014-03760C.
Ooshio T, Kobayashi R, Ikeda W, Miyata M, Fukumoto Y, Matsuzawa N, Ogita H, Takai Y (2010). Involvement of the interaction of afadin with ZO-1 in the formation of tight junctions in Madin-Darby canine kidney cells. J Biol Chem 285, 5003–5012.
Pimentel DR, Amin JK, Xiao L, Miller T, Viereck J, Oliver-Krasinski J, Baliga R, Wang J, Siwik DA, Singh K, *et al*. (2001). Reactive oxygen species mediate amplitude-dependent hypertrophic and apoptotic responses to mechanical stretch in cardiac myocytes. Circ Res 89, 453–460.
Ranieri VM, Suter PM, Tortorella C, De Tullio R, Dayer JM, Brienza A, Bruno F, Slutsky AS (1999). Effect of mechanical ventilation on inflammatory mediators in patients with acute respiratory distress syndrome: a randomized controlled trial. J Am Med Assoc 282, 54–61.
Rubenfeld GD, Caldwell E, Peabody E, Weaver J, Martin DP, Neff M, Stern EJ, Hudson LD (2005). Incidence and outcomes of acute lung injury. N Engl J Med 353, 1685–1693.
Sanchez-Esteban J, Wang Y, Cicchiello LA, Rubin LP (2002). Cyclic mechanical stretch inhibits cell proliferation and induces apoptosis in fetal rat lung fibroblasts. Am J Physiol Lung Cell Mol Physiol 282, L448–L456.
Severson EA, Parkos CA (2009). Mechanisms of outside-in signaling at the tight junction by junctional adhesion molecule A. Ann NY Acad Sci 1165, 10–18.
Shikata Y, Rios A, Kawkitinarong K, DePaola N, Garcia JG, Birukov KG (2005). Differential effects of shear stress and cyclic stretch on focal adhesion remodeling, site-specific FAK phosphorylation, and small GTPases in human lung endothelial cells. Exp Cell Res 304, 40–49.
Singleton PA, Chatchavalvanich S, Fu P, Xing J, Birukova AA, Fortune JA, Klibanov AM, Garcia JG, Birukov KG (2009). Akt-mediated transactivation of the S1P1 receptor in caveolin-enriched microdomains regulates endothelial barrier enhancement by oxidized phospholipids. Circ Res 104, 978–986.
Storck J, Zimmermann ER (1996). Regulation of the thrombin receptor response in human endothelial cells. Thromb Res 81, 121–131.
Takai Y, Nakanishi H (2003). Nectin and afadin: novel organizers of intercellular junctions. J Cell Sci 116, 17–27.
Tamada M, Sheetz MP, Sawada Y (2004). Activation of a signaling cascade by cytoskeleton stretch. Dev Cell 7, 709–718.
Tian X, Tian Y, Gawlak G, Meng F, Kawasaki Y, Akiyama T, Birukova AA (2015a). Asef controls vascular endothelial permeability and barrier recovery in the lung. Mol Biol Cell 26, 636–650.
Tian Y, Gawlak G, Shah AS, Higginbotham K, Tian X, Kawasaki Y, Akiyama T, Sacks DB, Birukova AA (2015b). Hepatocyte growth factor-induced Asef-IQGAP1 complex controls cytoskeletal remodeling and endothelial barrier. J Biol Chem 290, 4097–4109.
Tremblay L, Valenza F, Ribeiro SP, Li J, Slutsky AS (1997). Injurious ventilatory strategies increase cytokines and c-fos m-RNA expression in an isolated rat lung model. J Clin Invest 99, 944–952.
Villar J, Flores C, Mendez-Alvarez S (2003). Genetic susceptibility to acute lung injury. Crit Care Med 31, S272–S275.
Ware LB, Matthay MA (2000). The acute respiratory distress syndrome. N Engl J Med 342, 1334–1349.
Yan J, Li F, Ingram DA, Quilliam LA (2008). Rap1a is a key regulator of fibroblast growth factor 2-induced angiogenesis and together with Rap1b controls human endothelial cell functions. Mol Cell Biol 28, 5803–5810.
Yang G, Im HJ, Wang JH (2005). Repetitive mechanical stretching modulates IL-1β induced COX-2, MMP-1 expression, and PGE2 production in human patellar tendon fibroblasts. Gene 363, 166–172.